



Research paper

Fragment-based drug discovery of triazole inhibitors to block PDE δ -RAS protein-protein interaction

Danqi Chen^{a,1}, Yuehong Chen^{b,1}, Fulin Lian^{a,1}, Liu Chen^a, Yanlian Li^a, Danyan Cao^a, Xin Wang^a, Lin Chen^a, Jian Li^a, Tao Meng^a, Min Huang^{b,***}, Meiyu Geng^b, Jingkang Shen^a, Naixia Zhang^{a,**}, Bing Xiong^{a,*}

^a Department of Medicinal Chemistry, Shanghai Institute of Materia Medica, Chinese Academy of Sciences, 555 Zuchongzhi Road, Shanghai, 201203, China

^b Division of Anti-tumor Pharmacology, State Key Laboratory of Drug Research, Shanghai Institute of Materia Medica, Chinese Academy of Sciences, 555 Zuchongzhi Road, Shanghai, 201203, China

ARTICLE INFO

Article history:

Received 14 July 2018

Received in revised form

7 December 2018

Accepted 8 December 2018

Available online 11 December 2018

Keywords:

PDE δ -RAS

Fragment-based

Inhibitor

Protein-protein interaction

ABSTRACT

Although mutated Ras protein is well recognized as an important drug target, direct targeting Ras has proven to be a daunting task. Recent studies demonstrated that Ras protein needs PDE δ to relocate to plasma membrane to execute its signaling transduction function, which provides a new avenue for modulating the Ras protein. To find small molecules antagonizing the interactions between PDE δ and Ras, here we presented a successful application of fragment-based drug discovery of PDE δ inhibitors. Under the guidance of crystal structures, we are able to quickly optimize the initial fragment into highly potent inhibitors, with more than 2000-fold improvement in binding activity, which further adds to the arsenal towards the inhibition of Ras signaling in cancer therapy.

© 2018 Elsevier Masson SAS. All rights reserved.

1. Introduction

Mutational activation of the RAS oncogene products (HRAS, NRAS and KRAS) is a frequent event in human cancers [1]. Belonging to small GTPase family, Ras functions as a molecular switch in controlling extracellular growth signal transduction in many vital cellular processes such as cell differentiation, proliferation and survival. Through conformational transformation from an inactive GDP-bound state to an active GTP-bound state, Ras protein relays the signals from extracellular kinase receptors and interacts with various downstream effectors such as Raf, PI3K and Ral-GDS,

thereby triggering further cellular activities. Since its discovery in 1982, mutated Ras remains as an elusive anticancer target for more than three decades [2–5], and no candidates directly modulating Ras have entered into clinical trial. Several reasons account for this issue: 1) Ras proteins bind GDP or GTP with picomolar affinity, and the cellular concentrations of GDP and GTP are at micromolar level. This limits the development of GDP/GTP competitive inhibitors against Ras [6,7]. 2) The activities of Ras proteins are regulated by guanine nucleotide exchange factors (GEFs) and GTPase-activating proteins (GAPs). Although these protein-protein interactions (PPI) provide binding interfaces which could be targeted by small molecular antagonists, these potential binding sites are generally shallow and flat, and consequently challenges the design of Ras PPI inhibitors. Nevertheless, with the considerable efforts, researchers have discovered several potent inhibitors [8,9], especially the covalent inhibitors targeting small portions of mutated Ras containing cysteine at the vicinity of the binding sites [10,11].

The function of Ras depends on its intracellular localization at the plasma membrane [12–14]. After post-translational modification at the C-terminal hypervariable region of Ras protein at the endomembrane, a shuttling factor called PDE δ (the delta subunit of rod specific cyclic GMP phosphodiesterase) [15] binds to the modified C-terminus of Ras protein. By this process, PDE δ helps Ras

Abbreviations: EDC, 1-(3-Dimethylaminopropyl)-3-ethylcarbodiimide hydrochloride; DMF, *N,N*-Dimethylformamide; SEMCl, 2-(trimethylsilyl)ethoxymethyl chloride; DIEA, *N,N*-diisopropylethylamine; FBDD, Fragment-based drug discovery; ERK, Extracellular signal-regulated kinase; MAPK, Mitogen-activated protein kinase.

* Corresponding author.

** Corresponding author.

*** Corresponding author.

E-mail addresses: mhuang@simmm.ac.cn (M. Huang), nxzhong@simmm.ac.cn (N. Zhang), bxiong@simmm.ac.cn (B. Xiong).

¹ These authors contributed equally.

protein to leave the endomembrane and diffuse into different parts of cell. Next, with the help of small GTPase Arl2, the Ras protein dissociates from PDE δ and relocates to the plasma membrane through the electrostatic and hydrophobic interactions. On the basis of the critical role of PDE δ in transporting Ras proteins, Waldmann et al. utilized high throughput screening and structure-based optimization to discover a small molecule Deltarasin ($K_d = 38$ nM) interrupting the PDE δ -Ras interaction (Fig. 1) [16]. Further cellular and *in vivo* studies demonstrated that this compound could suppress Ras-related proliferation of human pancreatic ductal adenocarcinoma cells, therefore providing a novel strategy to modulate the Ras signaling pathway.

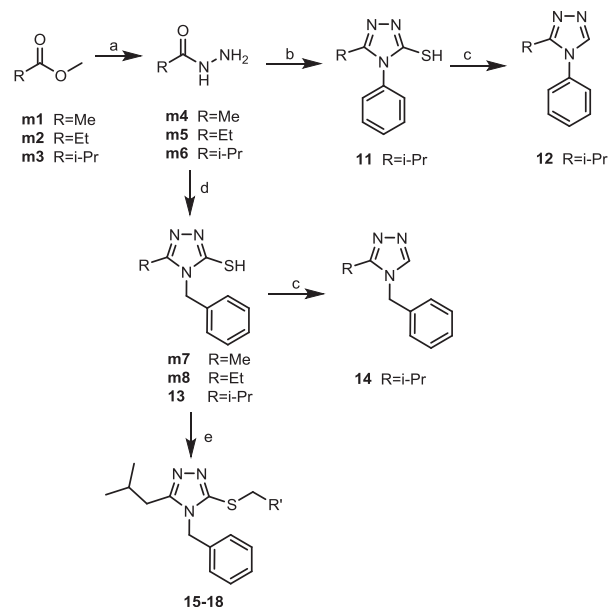
Encouraged by these appealing results, we were engaged in discovering new chemotypes of antagonist for PDE δ -Ras interaction. Using our fragment-based drug discovery (FBDD) platform [17,18], we were able to identify several fragment hits. Extensive co-crystallization and X-ray diffraction showed an interesting co-crystal structure containing one of the fragments, which underwent optimization and became nanomolar inhibitors. Together with the newly identified PDE δ inhibitors [19–22], current reported PDE δ -Ras antagonists will further add to the arsenal towards the inhibition of Ras signaling in cancer therapy.

1.1. Chemistry

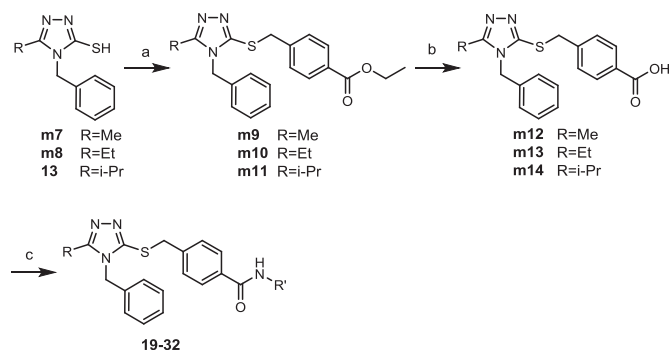
Commercially available methyl esters (**m1–m3**) were reacted with hydrazine monohydrate to form hydrazides (**m4–m6**), which underwent cyclization with isothiocyanates to give 1,2,4-triazole-3-thiols (**11**, **m7**, **m8** and **13**). The hydrosulfide groups of compounds (**11**, **13**) were removed by hydrogen peroxide to yield compound **12** and **14**. In other cases, compounds (**m7**, **m8**) were reacted with benzyl bromides to give compounds **15–18** (Scheme 1).

Compounds **m7**, **m8** and **13** were reacted with ethyl 4-(bromomethyl)benzoate to yield compounds **m9–m11**, which were hydrolyzed to give products **m12–m14**. These carboxylic acids were coupled with different amines to give compounds **19–32** (see Scheme 2).

The hydroxyl group of **m15** was protected using 2-(trimethylsilyl)ethoxymethyl chloride to give intermediate **m16**. Starting with **m16**, **m19** was obtained using the route described in Scheme



Scheme 1. Syntheses of compounds **15–18**. a) Hydrazine monohydrate, EtOH, reflux; b) phenyl isothiocyanate, K_2CO_3 , EtOH, reflux, 71% for two steps; c) HAc, 30% aq. H_2O_2 , CH_2Cl_2 , 35 °C to rt, 31–60%; d) benzyl isothiocyanate, K_2CO_3 , EtOH, reflux, 55–85%; e) benzyl bromides, Cs_2CO_3 , acetonitrile, rt, 68–97%.



Scheme 2. The syntheses of compounds **19–32**. a) Ethyl 4-(bromomethyl)benzoate, Cs_2CO_3 , acetonitrile, rt; b) LiOH, MeOH: H_2O (3:1), 60 °C to rt, 56–86% for two steps; c) amines, EDC, 4-dimethylaminopyridine, DMF, rt, 45–97%.

1. After deblocking, the hydroxyl group was coupled with methyl bromoacetate to yield **m21**, which was then hydrolyzed to **m22**. This compound was coupled with different amines to get compounds **33–39** (see Scheme 3).

As shown in Scheme 4, 3-(4-Methoxyphenyl)propanoic acid was condensed with benzylamine to give **m24**, which was treated with Lawesson reagent to yield **m25**. **M25** was reacted with **m17** to give the triazole **m26**. Compounds **40–43** were obtained from **m26** using the route described in Scheme 3.

2. Results and discussion

2.1. Hit finding

To increase the efficiency of lead discovery, fragment-based approach combines the advantages of random screening and structure-based rational drug design. Biophysical techniques, including NMR, X-ray crystallography and SPR, are the most commonly used screening and/or protein-compound complex characterization approaches in FBDD [23]. In current work, we

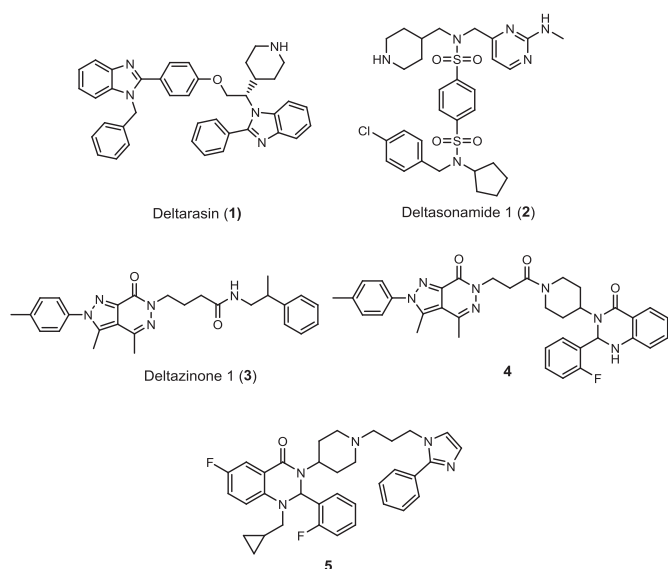
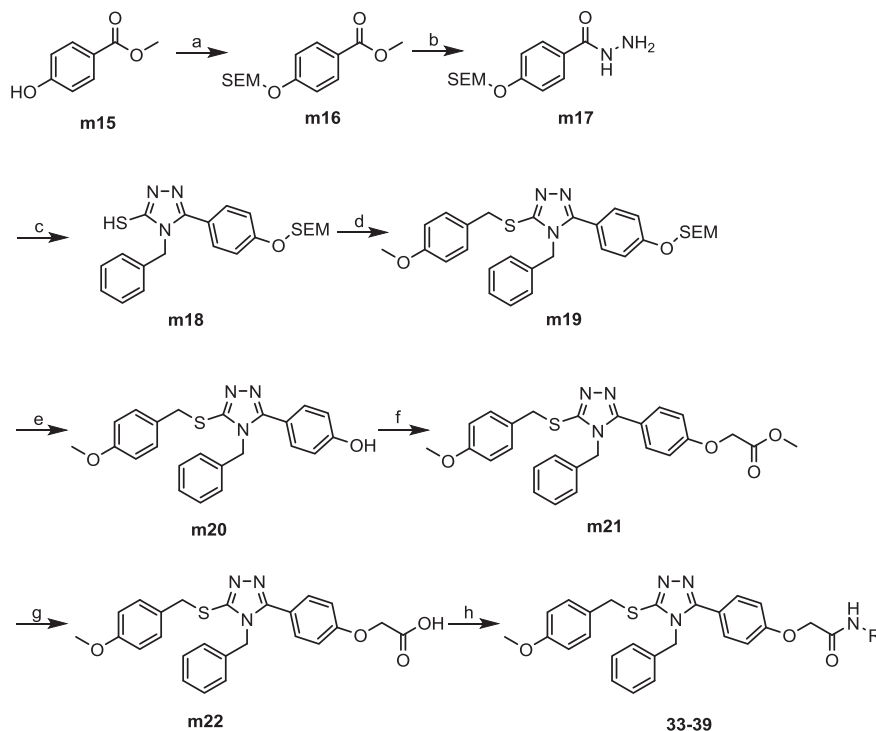
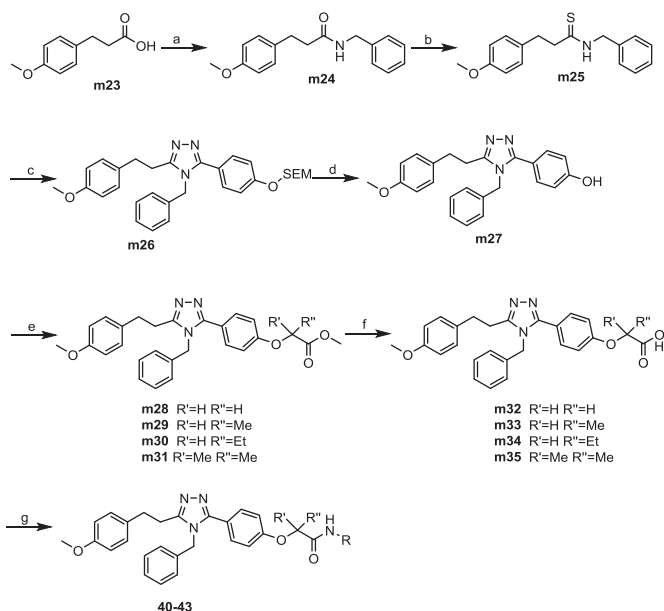


Fig. 1. Representative PDE δ -Ras inhibitors.



Scheme 3. The synthesis of compounds **33–39**. a) SEMCl, Cs₂CO₃, CH₃CN, rt, 77%; b) hydrazine hydrate, MeOH, reflux; c) benzyl isothiocyanate, sodium ethoxide, EtOH, reflux, 51% for two steps; d) 4-methoxybenzyl bromide, Cs₂CO₃, CH₃CN, rt, 62%; e) HCl/dioxane, rt, 93%; f) methyl bromoacetate, K₂CO₃, DMF, 55 °C, 87%; g) 1N NaOH, EtOH, rt, 88%; h) 1-hydroxybenzotriazole, EDC, DIEA, DMF, rt, 27–88%.



Scheme 4. The synthesis of compounds **40–43**. a) Benzylamine, EDC, 1-Hydroxybenzotriazole, DIEA, DMF, rt, 95%; b) Lawesson reagent, toluene, 110 °C, 53%; c) **m17**, HgOAc, HOAc, tetrahydrofuran, 0 °C, rt, 55%; d) HCl/dioxane, rt, 75%; e) substituted methyl bromoacetates, K₂CO₃, DIEA, 55 °C, 70%; f) 1N NaOH, EtOH, rt, 64%; g) 1-hydroxybenzotriazole, EDC, DIEA, DMF, rt, 26–53%.

employed saturation transfer difference (STD) and Carr Purcell Meiboom Gill (CPMG) for the primary NMR screening of 535 fragment compounds. After the primary combo (8–10 compounds per group without the overlap of characteristic ¹H NMR spectra) screening and the second round of single molecule re-examination,

five hits were identified (Fig. 2A), which gave the hit rate about 1%

To simultaneously verify the hit fragments and obtain the binding mode of fragments in the binding site of PDEδ, co-crystallization experiments were performed and fragment **1-H9** (5-(isopropylthio)-1-phenyl-1H-tetrazole) was found in the binding site of PDEδ. As shown in Fig. 2B, the tetrazole group forms several hydrogen bonds with the nearby polar residues Arg61 and Gln78. The isopropylthio group points to a hydrophobic subpocket constituted by residues Leu17, Leu38 and Phe133. And the phenyl group attached to the tetrazole is directed to the subpocket of Trp32 and Val49. Comparing 1-H9 with the cocystal structure of PDEδ bound to Deltarasin (Fig. 2C), the tetrazole group of fragment **1-H9** located at a similar position to the imidazole moiety of Deltarasin. In our crystal structure, a large room near the N² of the tetrazole was found and could be used for further optimization. Since tetrazole structure forbids further extension to this unoccupied subpocket, it was replaced with a triazole group by removing the N² in fragment **1-H9**. Meanwhile, the isopropylthio group was substituted by isobutyl group for synthesis convenience. According to this rational design, we synthesized new fragments to determine the core structure for further optimization (schemed in right side of Fig. 2C).

2.2. Scaffold modification and first round optimization

To check the replacement of N² of **1-H9** by a carbon atom, compound **12** and **14**, together with the intermediates **11** and **13**, were tested for their binding activities on PDEδ (Table 1) via fluorescence polarization-based (FP) assay. Briefly, the fluorescent ligand was synthesized by attaching 5-FIFC fluorescent fragment to the Atorvastatin. Final concentrations of PDEδ and fluorescent ligand were fixed to 20 nM; then viable concentration of ligands were added to the mixture and equilibrated in dark for 4 h at room

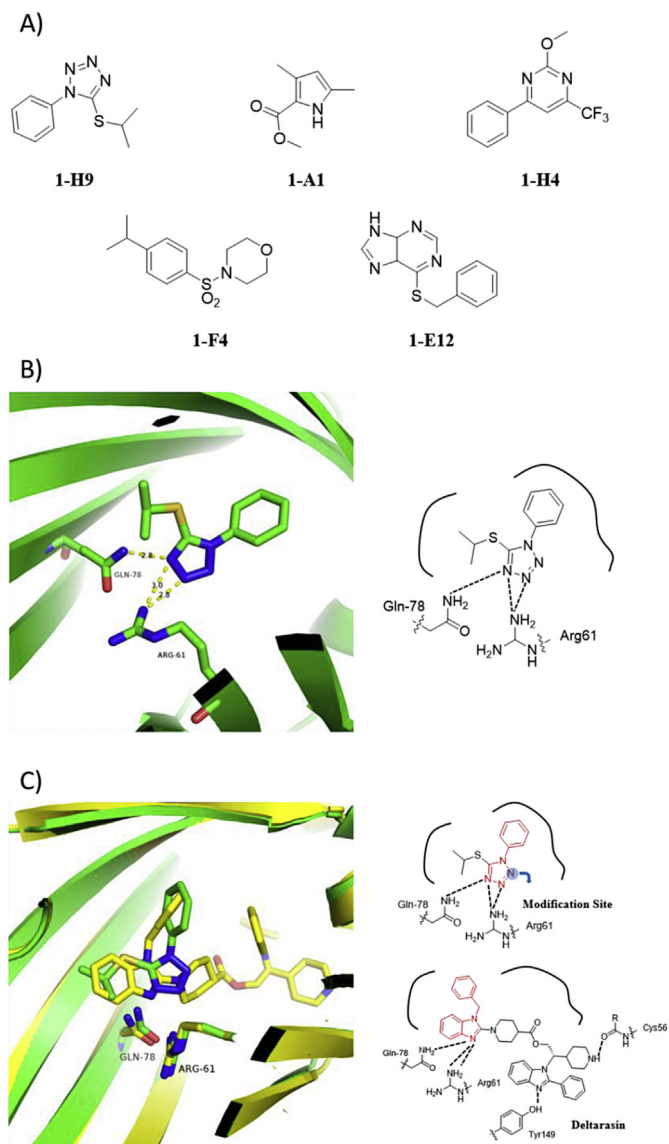


Fig. 2. The NMR fragment hits and co-crystal structures of inhibitors bound to PDE δ . A) Chemical structures of five NMR fragment hits. B) Co-crystal structure of fragment hit **1-H9** bound to PDE δ (PDB code: 5YAV) and the diagram of interactions between the fragment **1-H9** and the binding site of PDE δ . C) Superimpose co-crystal structures of fragment **1-H9** (colored in green) with Deltarasin (colored in yellow, PDB code: 4JVF), and the diagram of scaffold modification and optimization strategy.

temperature before measuring the fluorescence intensity. The results from FP assay showed that the activities of triazole compounds **12** and **14** were preserved. Therefore, the triazole scaffold could provide a new vector for optimization. Since there was only slight differences between compounds containing phenyl and benzyl groups (**12** and **14**), the benzyl group was adopted in further optimization.

Based on the superimposition of the cocrystal structures of Deltarasin and the fragment **1-H9**, we could identify that the fragment only occupied a small part of the binding pocket, which might be the reason for its weak binding activity on PDE δ . To increase the binding activity, we enlarged the fragment at the right side and synthesized compounds **15–18**, as shown in Table 1. These compounds showed increased inhibition on PDE δ with over 90% at 50 μ M when compared to 54% at 50 μ M of fragment **1-H9**. Since compound **16** with para-position of the benzyl group showed

Table 1

Binding activities of compounds **11–18** and fragment **1-H9** (**6**) on PDE δ .

Compd.	R	Inhibition%@50 μ M ^a	Inhibition%@1 μ M ^a
1-H9 (6)		54	ND ^b
11	–	44	ND
12	–	52	ND
13	–	10	ND
14	–	58	ND
15	Ph	96	21
16	4-OMe-Ph	94	46
17	3-OMe-Ph	97	29
18	4-CONH ₂ -Ph	93	17
Deltarasin	IC ₅₀ = 21 \pm 3 nM		

^a All assay data are reported as the average of at least two measurements.

^b ND: not determined.

higher activities than meta-substituted compound **17**, we further modified the molecules by keeping the isobutyl group at the left side and adding the substituents at the para-position of benzyl group on the right side.

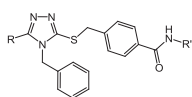
As shown in Table 2, amide derivatives **19–32** were evaluated. Most of these compounds showed significant improvement in their binding activities on PDE δ from μ M level to below 100 nM, which was much higher than compound **15**. Replacement of isobutyl group by methyl (**19**) or ethyl (**20**) indicated that the smaller the substitution was, the weaker the activity of compound towards PDE δ . It was also found that amides with substituted phenyls showed excellent activities and the IC₅₀ value of such type was lower than 70 nM. Placing the fluoro atom (**21**, **26–27**) or the trifluoromethyl group (**28–29**) at different positions of benzene group showed similar binding activities. Also, substitutions at the para-position including dimethylamino (**23**), methoxyl (**25**) or phenyl group (**24**) did not give distinct differences in activities. Together, these indicated that electronic property, size or substituting position might have little effect on inhibition activities. However, when the pyridyl was used to replace the phenyl ring, the activities decreased dramatically (**32**).

2.3. Revealing the binding mode and second round of optimization

According to the co-crystal structure of fragment **1-H9**, we knew that the isopropylthio motif in fragment **1-H9** occupied the left side of binding site. Therefore, we speculated that the isobutyl group in compounds **15–18** would still bind to the similar position as the isopropylthio group does in the crystal structure. Therefore, the substituted benzyl groups connecting to the sulfur atom should extend towards the right side of the cavity. However, after solving the co-crystal structure of compound **16** bound to PDE δ , we found that the binding mode was reversed (Fig. 3). As shown in Fig. 3, in reality, the isobutyl group situated at the middle of the binding cavity, while the substituted benzyl group extends to the left side and reaches to the boundary of the binding site, showing that the sulfur atom are almost at the same position.

On the basis of this surprising result, we designed a new series of inhibitors, in which 4-methoxybenzylthio was reserved, and the isobutyl group was modified to occupy the right side of the binding cavity. In analogy with Deltarasin, a phenyl ring substituted by hydroxyacetamide at 4-position was used to replace the isobutyl group and different amines were incorporated into amides. As

Table 2
Inhibition of compounds **19–32** on PDE δ .



Compd.	R	R'	IC ₅₀ (nM)	LE*
19	Me		540 ± 153	0.28
20	Et		137 ± 6	0.30
21	i-Bu		27 ± 5	0.31
22	i-Bu		35 ± 10	0.32
23	i-Bu		21 ± 6	0.30
24	i-Bu		39 ± 9	0.27
25	i-Bu		43 ± 4	0.29
26	i-Bu		33 ± 5	0.31
27	i-Bu		37 ± 7	0.31
28	i-Bu		64 ± 4	0.27
29	i-Bu		61 ± 23	0.27
30	i-Bu		113 ± 14	0.26
31	i-Bu		30 ± 2	0.32
32	i-Bu		1008 ± 206	0.25

* LE: ligand efficiency.

shown in Table 3, the new series maintained binding activities on PDE δ . When R group was *N*, *N*-dimethyl substituted phenyl ring (**33**), heterocyclic or aliphatic rings, compounds **34–37** showed excellent binding activities of IC₅₀ below 50 nM. However, when R was hydrophilic amine chains, compounds **38–39** showed activities of micromolar level. This might be due to the negative interaction of the polar groups in the binding site.

Since the sulfur atom was prone to oxidation and it had no direct interaction in the crystal structure, we synthesized the compound **40**, replacing the sulfur atom with carbon. Meanwhile, labile metabolic sites including the methylene group between the carbonyl and the hydroxyl group were modified to give compounds **41–43** by adding small blocking groups at the corresponding position. As shown in Table 4, when the sulfur atom was replaced with carbon atom, the binding activity remained compared with compound **35**. When substituents were introduced to the methylene group, the compounds (**41–43**) also retained the potent binding activities, indicating that the introduced small groups did not perturb the binding conformation.

2.4. Cellular activity

On the basis of the FP assay results, we next tested the cellular

activity of the compounds that showed good binding activity to PDE δ . Non-small cell lung cancer A549 cell line bearing KRAS G12S mutation was selected for the assay as it showed growth dependency on PDE δ (data not shown). Cell viability was measured by the SRB assay. Indeed, most of the tested compounds, except for compounds **41**, **42** and **43**, moderately inhibited the proliferation of A549 cells with IC₅₀ value of 10–36 μ M (Table 5). Consistently, this potency largely reflected the sensitivity of this cell line to PDE δ depletion. We also noticed that the potency of Deltarasin was relatively higher than other tested compounds, which may echo the recent publication pointing out its off-target effects beyond KRAS signaling [19].

To confirm that the cellular activity of the tested compounds came from the inhibition of KRAS signaling, we monitored the MAPK signaling in A549 cells upon the treatment of the selected compounds. As shown in Fig. 4, p-RAF and p-ERK, the key signaling molecules in the MAPK pathway were inhibited by these compounds. Importantly, for compound **27**, **30**, **34**, their potency of reducing the MAPK signaling accorded with their anti-proliferative activity.

We also examined p-S6K, which was often considered as a surrogate marker of PDE δ function. Rheb is a Ras-related farnesylated protein that binds to PDE δ to activate the mTOR and the downstream p-S6K. Intriguingly, the tested compounds were more potent towards MAPK signaling than p-S6K, and this is different from the behavior of Deltarasin. This could indicate the selectivity of these compounds towards the MAPK signaling (Fig. 4).

During our fragment-based development of PDE δ -Ras inhibitors, Papke et al. [4] discovered that deltazinone **1** (**3**) was a more selective inhibitor than Deltarasin. This study indicated that Deltarasin could bind to several GPCRs, ion channels and transporters, which accounted for its 'switch-like' behaviors in the cellular growth inhibition assay as well as its off-target cytotoxicity. Similar to our inhibitors, deltazinone **1** required at least 10 μ M concentration to show effects in cell-based assays. The newly reported deltasonamide **1** (**2**) demonstrated a much higher affinity ($K_D = 203$ pM) as it formed several additional hydrogen bonding interactions with PDE δ . Proportionally, the binding activity of deltasonamide **1** increased more than 10 folds than that of deltazinone **1**. Therefore, the cellular activity of deltasonamide **1** demonstrated the IC₅₀ value of 0.75 μ M, which is about 10–20 fold improvement than deltazinone **1**. Clearly, there was a large gap between the binding activity and the cellular activity, and the reason should come from target specific issues. As revealed by Martin-Gago et al. Arl2 binding to PDE δ will trigger a fast release of inhibitors from PDE δ [20]. Detailed analysis of Arl2-PDE δ complex crystal structure revealed that Arl2 bound to the back of β -sheet at least 10 Å from the inhibitor binding site (Fig. S1) [24]. Recently, two series of quinazolinone based PDE δ inhibitors were identified with structure-based and fragment-based drug design methods, which all demonstrated excellent binding activities but with similar weak cellular activities [21,22]. Together with these structural and SAR knowledges, we thought that currently designed PDE δ inhibitors could not prevent the binding of Arl2, and would show similar tendency of lower efficiency in cellular content, although they demonstrated very potent binding activity to PDE δ . Besides, as reported by Waldmann et al. [20], PDE δ needs to be completely inhibited to relocalize KRAS to endomembranes, as even a small pool of uninhibited, free PDE δ is sufficient to reinstate plasma membrane localization of KRAS. These further increased the difficulty for developing cellular potent PDE δ inhibitors. The discrepancy between molecular and cellular activity among the tested compounds, such as 30, 34 versus 27 may stem from the fact that PDE δ is required for the membrane association of quite a few proteins beyond KRAS, including KRAS4b, RHEB, RAB23, CDC42 and

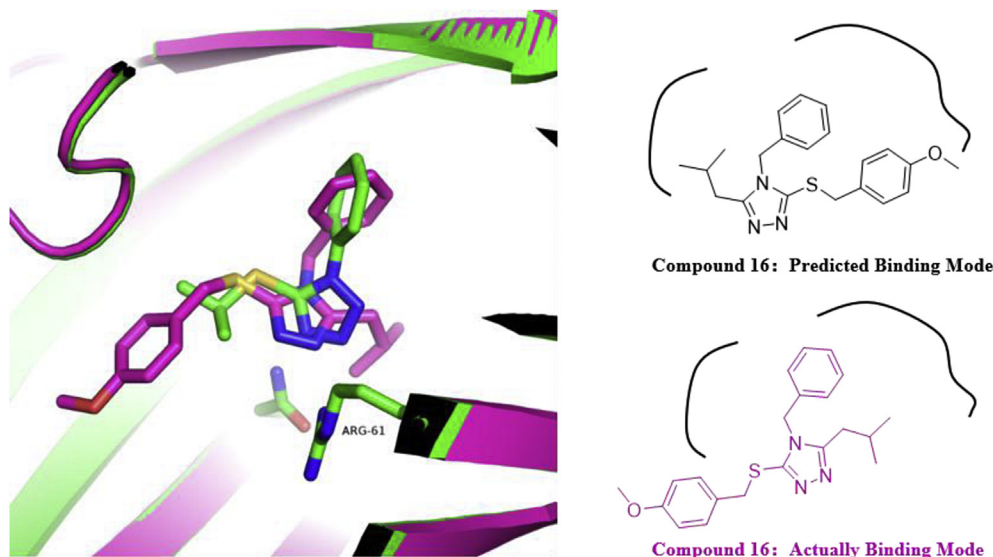
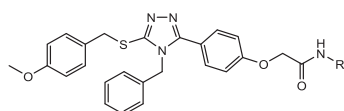


Fig. 3. Superimposition of the co-crystal structures of compound **16** bound to PDE δ (PDB code: 5YAW, colored in magenta) and the fragment 1-H9 bound to PDE δ (PDB code: 5YAV, colored in green) diagram of the predicted binding conformation (black) and actually solved binding mode (magenta). (For interpretation of the references to color in this figure legend, the reader is referred to the Web version of this article.)

Table 3
Inhibition of compounds **33–39** on PDE δ .



Compd.	R	IC ₅₀ (nM)	LE ^a
33		41.1 ± 16.5	0.25
34		25.0 ± 11.4	0.27
35		27.3 ± 1.7	0.27
36		40.3 ± 12.0	0.26
37		24.0 ± 6.9	0.27
38		50.39@1μ; M	
39		45.37@1μ; M	

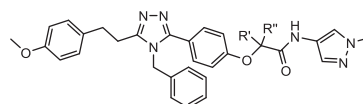
^a LE: ligand efficiency.

CNP [25,26]. The interfered functions of these proteins may account for the dissociation between PDE δ /KRAS signaling disruption and the cell growth inhibition in the KRAS mutant cell context. All these complexities of PDE δ -associated proteins may impose a challenge and opportunity for PDE δ -targeted anticancer drug discovery.

3. Conclusion

In summary, to discover new chemotype of PDE δ -Ras PPI antagonist, we employed the fragment-based drug discovery approach to identify five promising fragments from the ligand-based NMR screening. On the basis of the co-crystal structure from one of the fragments, we carried out the SAR elaboration by

Table 4
Inhibition of compounds **40–43** on PDE δ .



Compd.	R'	R''	IC ₅₀ (nM)	LE ^a
40	H	H	40.9 ± 12.4	0.27
41	H	Me	25.2 ± 4.0	0.27
42	H	Et	26.4 ± 4.4	0.26
43	Me	Me	33.6 ± 2.8	0.26

* LE: ligand efficiency.

Table 5
Antiproliferative activity of selected compounds in A549 cells.

Compd.	A549 IC ₅₀ (μM)
27	20.3 ± 0.3
30	10.3 ± 0.3
31	32.6 ± 0.6
33	17.1 ± 0.3
34	11.3 ± 0.4
35	36.0 ± 0.8
36	18.3 ± 2.2
37	19.3 ± 0.5
40	24.1 ± 1.7
41	>50
42	>50
43	>50
Deltarasin	6.4 ± 0.2

using the information from Deltarasin binding analysis. Thereby, we were able to quickly enhance the binding activity about 1000 folds. After solving the crystal structure of one of the potent inhibitor **16**, we were surprised by the real binding mode, which was distinct from our prediction. Thus, we designed and synthesized next round of compounds to investigate the SAR as well as to optimize the metabolic stability. Further cellular activity study

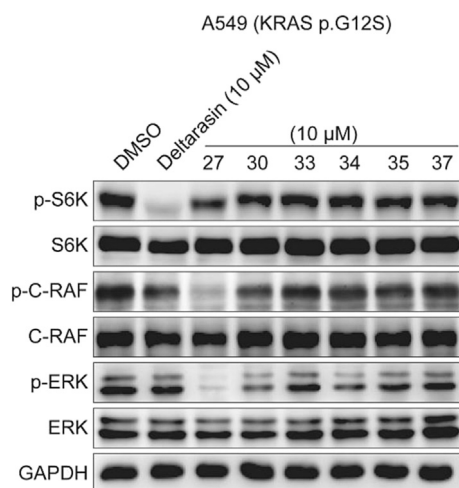


Fig. 4. The impact of selected compounds on KRAS signaling in A549 cells. A549 cells were treated with indicated compounds overnight and the signaling change was examined using immunoblotting.

confirmed that blocking the PDE δ -Ras interaction can reduce the activity of downstream of Ras signaling, although the anti-proliferative activity still remains at micromolar level. Nevertheless, as a successful application of FBDD, this study provided novel PDE δ inhibitors for further investigations.

4. Experimental section

Reagents (chemicals) were purchased from Aldrich (St. Louis, MO, USA), Adamas-beta (Shanghai, China), Shao-yuan (Shanghai, China), Bide Pharmatech (Shanghai, China) and Shanghai Chemical Reagent Company (Shanghai, China) and were used without further purification. Analytical thin-layer chromatography was performed on HSGF 254 (150–200 mm thickness; Yantai Huiyou Company, Yantai, Shandong, China). ^1H NMR (300 MHz or 400 MHz) spectra were recorded on a Varian Mercury-300 or 400 High Performance Digital FT-NMR with TMS as an internal standard. HPLC analysis was performed using a Gilson HPLC system with UV detection at 214 and 254 nm. LC–MS spectra were obtained on an LCQ Deca XP ion trap mass spectrometer (Thermo-Finnigan, San Jose, CA, USA). Accurate mass measurements were carried out on a Q-TOF ultima Globe mass spectrometer (Micromass, Manchester, UK).

5-Isobutyl-4-phenyl-4H-1,2,4-triazole-3-thiol (11). Methyl 3-methylbutanoate (10 g, 86.2 mmol) was added to hydrazine monohydrate (11 g, 343.8 mmol) in 50 mL of ethanol under ice bath. The mixture was refluxed overnight under N_2 and concentrate to dryness to give the intermediate **m6** as a white wax, which was used in the next step without purification. Compound **m6** (580 mg, 5 mmol) and phenyl isothiocyanate (675 mg, 5 mmol) were dissolved in 8 mL of EtOH and refluxed for 2 h. The mixture was cooled down and filtered. The solid was added to 8 mL of 1 N aq. NaOH and refluxed for another 2 h. The mixture was cooled down and neutralized by 1 N aq. HCl. The resulting solid was filtered, washed with water, and dried in vacuum to give the product as a white solid (830 mg, total yield 71%). ^1H NMR (400 MHz, Chloroform-*d*) δ 11.54 (s, 1H), 7.63–7.50 (m, 3H), 7.35–7.27 (m, 2H), 2.37 (d, $J = 7.3$ Hz, 2H), 1.95–1.80 (m, 1H), 0.88 (d, $J = 6.6$ Hz, 6H). ^{13}C NMR (126 MHz, DMSO) δ 168.02, 151.79, 134.30, 129.92, 128.76, 34.45, 26.00, 22.45. HPLC $t_{\text{R}} = 2.97$ min, purity: 98.93%. MS (ESI): m/z 234 $[\text{M}+\text{H}]^+$.

3-Isobutyl-4-phenyl-4H-1,2,4-triazole (12). Compound **11** (100 mg, 0.43 mmol) was suspended in 6 mL of CH_2Cl_2 , cooled to 0–5 $^\circ\text{C}$ and treated with a solution of 30% aq. H_2O_2 (0.12 mL) in

0.7 mL of acetic acid dropwise. After being stirred for 1 h at room temperature, the mixture was diluted with CH_2Cl_2 and washed with 1 N aq. NaOH. The organic layer was separated, dried with Na_2SO_4 , concentrated, and purified with silica gel chromatography (CH_2Cl_2 : MeOH 20:1) to give the product **12** as a white solid (52 mg, yield 60%). ^1H NMR (400 MHz, Chloroform-*d*) δ 8.19 (s, 1H), 7.60–7.48 (m, 3H), 7.33–7.24 (m, 2H), 2.61 (d, $J = 7.3$ Hz, 2H), 2.12–1.96 (m, 1H), 0.89 (d, $J = 6.7$ Hz, 6H). ^{13}C NMR (126 MHz, DMSO) δ 152.87, 144.41, 134.58, 130.29, 129.61, 126.24, 33.26, 27.10, 22.59. HPLC $t_{\text{R}} = 2.39$ min, purity: 97.64%. MS (ESI): m/z 202 $[\text{M}+\text{H}]^+$. HRMS (ESI+) calcd for $\text{C}_{12}\text{H}_{15}\text{N}_3\text{Na}[\text{M}+\text{Na}]$ 224.1158, found 224.1152.

4-Benzyl-5-methyl-4H-1,2,4-triazole-3-thiol (m7). Methyl acetate (1 g, 13.51 mmol) was added to hydrazine monohydrate (2.6 mL, 53.56 mmol) in 10 mL ethanol under ice bath. The mixture was refluxed overnight under N_2 and concentrate to dryness to give the product **m4** as white wax, which was used in the next step without purification. Compound **m4** (680 mg, 9.2 mmol) and benzyl isothiocyanate (1.37 g, 9.2 mmol) were dissolved in 10 mL EtOH and refluxed for 2 h. The mixture was cooled down, added K_2CO_3 (1.27 g, 9.2 mmol) and refluxed for another 1 h. The mixture was cooled down to room temperature and neutralized by 1N HCl. The resulting solid was filtered, washed with water and ether, and dried in vacuum to get the product as white solid (1.6 g, total yield 85%). ^1H NMR (400 MHz, Chloroform-*d*) δ 7.41–7.26 (m, 5H), 5.26 (s, 2H), 2.23 (s, 3H). MS (ESI): m/z 206 $[\text{M}+\text{H}]^+$.

4-Benzyl-5-ethyl-4H-1,2,4-triazole-3-thiol (m8). Prepared by the same method as compound **m7** starting with methyl propionate instead of methyl acetate. White solid, total yield 55%. ^1H NMR (400 MHz, Chloroform-*d*) δ 11.64 (s, 1H), 7.40–7.25 (m, 5H), 5.27 (s, 2H), 2.50 (q, $J = 7.5$ Hz, 2H), 1.21 (t, $J = 7.4$ Hz, 3H). MS (ESI): m/z 220 $[\text{M}+\text{H}]^+$.

4-Benzyl-5-isobutyl-4H-1,2,4-triazole-3-thiol (13). Prepared by the same method as compound **m7** using compound **m6** instead of **m4**. White solid, yield 69%. ^1H NMR (400 MHz, Chloroform-*d*) δ 12.13 (s, 1H), 7.41–7.23 (m, 5H), 5.28 (s, 2H), 2.37 (d, $J = 7.2$ Hz, 2H), 2.03–1.88 (m, 1H), 0.90 (d, $J = 6.6$ Hz, 6H). ^{13}C NMR (126 MHz, DMSO) δ 167.54, 152.12, 136.38, 129.12, 128.17, 127.33, 46.06, 34.03, 26.04, 22.43. HPLC $t_{\text{R}} = 3.17$ min, purity: 100%. MS (ESI): m/z 248 $[\text{M}+\text{H}]^+$. HRMS (ESI+) calcd for $\text{C}_{13}\text{H}_{18}\text{N}_3\text{S}[\text{M}+\text{H}]$ 248.1216, found 248.1217.

4-Benzyl-3-isobutyl-4H-1,2,4-triazole (14). Compound **13** (400 mg, 1.62 mmol) was suspended in 3 mL CH_2Cl_2 and added 0.12 mL acetic acid. The mixture was warmed to 35 $^\circ\text{C}$ and treated with a solution of 30% aq. H_2O_2 (aq. 0.12 mL) by dropwise and stirred at room temperature for 0.5 h. The reaction was adjusted to pH > 10 by 10% NaOH and the mixture was extracted by ethyl acetate. The organic layer was washed with brine, dried with Na_2SO_4 , concentrated and purified with sil gel chromatography (CH_2Cl_2 : MeOH 20:1) to get the product as yellow wax (110 mg, yield 31%). ^1H NMR (400 MHz, Chloroform-*d*) δ 8.06 (s, 1H), 7.43–7.31 (m, 3H), 7.13–7.05 (m, 2H), 5.09 (s, 2H), 2.57 (d, $J = 7.3$ Hz, 2H), 2.20–2.04 (m, 2H), 0.97 (d, $J = 6.6$ Hz, 6H). ^{13}C NMR (126 MHz, DMSO) δ 153.18, 144.65, 136.89, 129.27, 128.35, 127.55, 47.09, 32.82, 27.11, 22.61. HPLC $t_{\text{R}} = 2.49$ min, purity: 100%. MS (ESI): m/z 216 $[\text{M}+\text{H}]^+$. HRMS (ESI+) calcd for $\text{C}_{13}\text{H}_{17}\text{N}_3\text{Na}[\text{M}+\text{Na}]$ 238.1315, found 283.1318.

General procedure A for compounds **15–18**. Compound **13** (1 eq.), benzyl bromides (1 eq.) and Cs_2CO_3 (1.1 eq.) were stirred overnight in acetonitrile. The mixture was diluted with ethyl acetate. The organic layer was washed with brine, dried with Na_2SO_4 , concentrated and purified with sil gel chromatography (CH_2Cl_2 : MeOH 25:1) to get the product.

4-Benzyl-3-(benzylthio)-5-isobutyl-4H-1,2,4-triazole (15). Using benzyl bromide. Yellow thick oil, yield 84%. ^1H NMR (400 MHz, Chloroform-*d*) δ 7.31–7.21 (m, 8H), 6.92–6.83 (m, 2H), 4.78 (s, 2H),

4.32 (s, 2H), 2.44 (d, $J = 7.3$ Hz, 2H), 2.09–1.95 (m, 1H), 0.91 (d, $J = 6.6$ Hz, 6H). HPLC $t_R = 3.29$ min, purity: 100%. MS (ESI): m/z 338 $[M+H]^+$.

4-Benzyl-3-isobutyl-5-((4-methoxybenzyl)thio)-4H-1,2,4-triazole (**16**). Using 1-(bromomethyl)-4-methoxybenzene as the benzyl bromide. Yellow thick oil, yield 81%. 1H NMR (400 MHz, Chloroform- d) δ 7.31–7.23 (m, 3H), 7.20–7.12 (m, 2H), 6.87 (dd, $J = 6.6, 2.9$ Hz, 2H), 6.83–6.74 (m, 2H), 4.83 (s, 2H), 4.29 (s, 2H), 3.78 (s, 3H), 2.44 (d, $J = 7.2$ Hz, 2H), 2.09–1.94 (m, 1H), 0.91 (d, $J = 6.6$ Hz, 7H). HPLC $t_R = 3.42$ min, purity: 95.19%. MS (ESI): m/z 368 $[M+H]^+$.

4-Benzyl-3-isobutyl-5-((3-methoxybenzyl)thio)-4H-1,2,4-triazole (**17**). Using 1-(bromomethyl)-3-methoxybenzene as the benzyl bromide. Yellow thick oil, yield 90%. 1H NMR (400 MHz, Chloroform- d) δ 7.32–7.27 (m, 4H), 6.92–6.77 (m, 5H), 4.83 (s, 2H), 4.30 (s, 2H), 3.75 (s, 3H), 2.45 (d, $J = 7.1$ Hz, 2H), 2.07–1.95 (m, 1H), 0.91 (d, $J = 6.6$ Hz, 6H). ^{13}C NMR (126 MHz, DMSO) δ 159.67, 155.57, 149.05, 139.15, 136.22, 129.97, 129.22, 128.22, 126.79, 121.53, 114.84, 113.54, 55.44, 46.53, 38.07, 33.65, 26.99. HPLC $t_R = 3.30$ min, purity: 100%. MS (ESI): m/z 368 $[M+H]^+$.

4-(((4-Benzyl-5-isobutyl-4H-1,2,4-triazol-3-yl)thio)methyl)benzamide (**18**). Using 4-(bromomethyl)benzamide as the benzyl bromide. White wax, yield 71%. 1H NMR (400 MHz, Chloroform- d) δ 7.77–7.69 (m, 2H), 7.38–7.33 (m, 2H), 7.31–7.27 (m, 3H), 6.87 (m, 2H), 6.38–6.32 (m, 1H), 5.81 (s, 1H), 4.87 (s, 2H), 4.35 (s, 2H), 2.44 (d, $J = 7.3$ Hz, 2H), 2.09–1.93 (m, 1H), 0.90 (d, $J = 6.7$ Hz, 6H). ^{13}C NMR (126 MHz, DMSO) δ 167.91, 155.62, 148.84, 141.08, 136.17, 133.77, 129.21, 128.22, 128.06, 126.78, 46.58, 37.48, 33.63, 26.96, 22.55. HPLC $t_R = 2.79$ min, purity: 98.11%. MS (ESI): m/z 381 $[M+H]^+$.

4-(((4-Benzyl-5-methyl-4H-1,2,4-triazol-3-yl)thio)methyl)benzoic acid (**m12**). The intermediate **m9** was prepared using general procedure A by compound **m7** coupling with ethyl 4-(bromomethyl)benzoate. The crude product was dissolved in MeOH: H₂O (3:1) 4 mL and added LiOH 800 mg. The mixture was stirred at 60 °C for 5 h and then overnight at room temperature. The reaction was diluted with water and washed with ethyl acetate. The aqueous layer was adjusted to pH3 by 1N HCl and extracted with ethyl acetate. The organic layer was washed with brine, dried with Na₂SO₄, concentrated to get the product as pale yellow solid 582 mg, total yield 70%. 1H NMR (400 MHz, DMSO- d_6) δ 12.97–12.88 (m, 1H), 7.86 (d, $J = 8.0$ Hz, 2H), 7.41 (d, $J = 8.0$ Hz, 2H), 7.30 (d, $J = 6.2$ Hz, 3H), 7.00–6.93 (m, 2H), 5.06 (s, 2H), 4.37 (s, 2H), 2.25 (d, $J = 7.1$ Hz, 3H). MS (ESI): m/z 340 $[M+H]^+$.

4-(((4-Benzyl-5-ethyl-4H-1,2,4-triazol-3-yl)thio)methyl)benzoic acid (**m13**). Prepared by the same method of compound **m12** starting with compound **m8**. White solid, yield 56%. 1H NMR (400 MHz, DMSO- d_6) δ 12.97 (s, 1H), 7.89–7.82 (m, 2H), 7.44–7.37 (m, 2H), 7.35–7.23 (m, 3H), 6.98–6.90 (m, 2H), 5.05 (s, 2H), 4.38 (s, 2H), 2.59 (q, $J = 7.5$ Hz, 2H), 1.12 (t, $J = 7.5$ Hz, 3H). MS (ESI): m/z 354 $[M+H]^+$.

4-(((4-Benzyl-5-isobutyl-4H-1,2,4-triazol-3-yl)thio)methyl)benzoic acid (**m14**). Prepared by the same method of compound **m12** starting with compound **13**. Pale yellow solid, yield 86%. 1H NMR (400 MHz, DMSO- d_6) δ 7.88–7.80 (m, 2H), 7.42–7.34 (m, 2H), 7.34–7.22 (m, 3H), 6.95–6.88 (m, 2H), 5.02 (s, 2H), 4.36 (s, 2H), 2.46 (d, $J = 7.2$ Hz, 2H), 1.93–1.78 (m, 1H), 0.82 (d, $J = 6.6$ Hz, 6H). ^{13}C NMR (126 MHz, DMSO) δ 167.49, 155.66, 148.71, 142.87, 136.17, 130.37, 129.87, 129.50, 129.20, 128.22, 126.77, 46.55, 37.53, 33.60, 26.99, 22.53. MS (ESI): m/z 382 $[M+H]^+$. HRMS (ESI+) calcd for C₂₁H₂₄N₃O₂S $[M+H]$ 382.1584, found 382.1573.

General procedure B for compounds **19–32**. The acids (**m12–m14**, 1 eq.), amines (2 eq.), 1-Ethyl-3-(3-dimethylaminopropyl)carbodiimide hydrochloride (1 eq.) and 4-dimethylaminopyridine (0.1 eq.) were dissolved in N,N-dimethylformamide and the mixture was stirred at room temperature overnight. The solvent

was removed by vacuum and the residue was purified by sil gel chromatography (CH₂Cl₂: MeOH 20:1) to get the corresponding product.

4-(((4-Benzyl-5-methyl-4H-1,2,4-triazol-3-yl)thio)methyl)-N-(4-fluorophenyl)benzamide (**19**). Using compound **m12** as the acid and 4-fluoroaniline as the amine. Yellow solid, yield 46%. 1H NMR (400 MHz, DMSO- d_6) δ 10.27 (s, 1H), 7.86 (d, $J = 8.2$ Hz, 2H), 7.81–7.75 (m, 2H), 7.45 (d, $J = 8.1$ Hz, 2H), 7.36–7.25 (m, 3H), 7.19 (t, $J = 8.9$ Hz, 2H), 6.98 (dd, $J = 7.6, 1.8$ Hz, 2H), 5.07 (s, 2H), 4.38 (s, 2H), 2.27 (s, 3H). HPLC $t_R = 3.11$ min, purity: 95.25%. MS (ESI): m/z 433 $[M+H]^+$.

4-(((4-benzyl-5-ethyl-4H-1,2,4-triazol-3-yl)thio)methyl)-N-(4-fluorophenyl)benzamide (**20**). Using compound **m13** as the acid and 4-fluoroaniline as the amine. White solid, yield 53%. 1H NMR (400 MHz, DMSO- d_6) δ 10.26 (s, 1H), 7.87 (d, $J = 8.3$ Hz, 2H), 7.82–7.73 (m, 2H), 7.45 (d, $J = 8.3$ Hz, 2H), 7.35–7.25 (m, 3H), 7.19 (t, $J = 8.9$ Hz, 2H), 6.99–6.92 (m, 2H), 5.07 (s, 2H), 4.39 (s, 2H), 2.59 (q, $J = 7.5$ Hz, 2H), 1.12 (t, $J = 7.5$ Hz, 3H). ^{13}C NMR (126 MHz, DMSO) δ 165.51, 157.35, 149.00, 141.61, 136.07, 134.23, 129.38, 129.28, 128.23, 126.91, 122.66, 115.73, 115.56, 46.55, 37.18, 18.62, 11.56. HPLC $t_R = 3.27$ min, purity: 100%. MS (ESI): m/z 447 $[M+H]^+$.

4-(((4-benzyl-5-isobutyl-4H-1,2,4-triazol-3-yl)thio)methyl)-N-(4-fluorophenyl)benzamide (**21**). Using compound **m14** as the acid and 4-fluoroaniline as the amine. Off-white solid, yield 48%. 1H NMR (400 MHz, DMSO- d_6) δ 10.26 (s, 1H), 7.86 (d, $J = 8.2$ Hz, 2H), 7.83–7.73 (m, 2H), 7.43 (d, $J = 8.2$ Hz, 2H), 7.36–7.23 (m, 3H), 7.19 (t, $J = 8.9$ Hz, 2H), 6.98–6.90 (m, 2H), 5.06 (s, 2H), 4.38 (s, 2H), 2.47 (d, $J = 7.2$ Hz, 2H), 1.95–1.79 (m, 1H), 0.83 (d, $J = 6.6$ Hz, 6H). ^{13}C NMR (126 MHz, DMSO) δ 165.47, 159.70, 157.79, 155.67, 148.83, 141.58, 136.17, 135.92, 134.19, 129.37, 129.24, 128.25, 128.22, 126.80, 122.68, 122.61, 115.73, 115.56, 46.60, 37.35, 33.62, 26.98, 22.56. HPLC $t_R = 3.37$ min, purity: 97.71%. MS (ESI): m/z 475 $[M+H]^+$. HRMS (ESI+) calcd for C₂₇H₂₈FN₄OS $[M+H]$ 475.1962, found 475.1976.

4-(((4-benzyl-5-isobutyl-4H-1,2,4-triazol-3-yl)thio)methyl)-N-phenylbenzamide (**22**). Using compound **m14** as the acid and aniline as the amine. White solid, yield 50%. 1H NMR (400 MHz, DMSO- d_6) δ 10.20 (s, 1H), 7.87 (d, $J = 8.5$ Hz, 2H), 7.76 (d, $J = 8.1$ Hz, 2H), 7.43 (d, $J = 8.1$ Hz, 2H), 7.38–7.26 (m, 5H), 7.10 (t, $J = 7.6$ Hz, 1H), 6.94 (d, $J = 6.8$ Hz, 2H), 5.05 (s, 2H), 4.38 (s, 2H), 2.47 (d, $J = 7.1$ Hz, 2H), 1.93–1.83 (m, 1H), 0.83 (d, $J = 6.5$ Hz, 6H). HPLC $t_R = 3.35$ min, purity: 98.92%. MS (ESI): m/z 457 $[M+H]^+$. HRMS (ESI+) calcd for C₂₇H₂₉N₄O₂S $[M+H]$ 457.2057, found 457.2055.

4-(((4-benzyl-5-isobutyl-4H-1,2,4-triazol-3-yl)thio)methyl)-N-(4-(dimethylamino)phenyl)benzamide (**23**). Using compound **m14** as the acid and N,N-dimethylbenzene-1,4-diamine as the amine. Brown solid, yield 78%. 1H NMR (400 MHz, DMSO- d_6) δ 9.94 (s, 1H), 7.85 (d, $J = 8.2$ Hz, 2H), 7.56 (d, $J = 9.0$ Hz, 2H), 7.40 (d, $J = 8.1$ Hz, 2H), 7.36–7.23 (m, 3H), 6.97–6.90 (m, 2H), 6.72 (d, $J = 9.1$ Hz, 2H), 5.05 (s, 2H), 4.37 (s, 2H), 2.87 (s, 6H), 2.47 (d, $J = 7.2$ Hz, 2H), 1.93–1.79 (m, 1H), 0.83 (d, $J = 6.6$ Hz, 6H). ^{13}C NMR (126 MHz, DMSO) δ 164.73, 155.66, 148.86, 147.79, 141.07, 136.19, 134.65, 129.27, 129.24, 128.25, 128.06, 126.80, 122.30, 112.91, 46.60, 40.93, 37.43, 33.63, 26.98, 22.57. HPLC $t_R = 2.82$ min, purity: 99.36%. MS (ESI): m/z 500 $[M+H]^+$. HRMS (ESI+) calcd for C₂₉H₃₃N₅NaOS $[M+Na]$ 522.2298, found 522.2297.

N-([1,1'-biphenyl]-4-yl)-4-(((4-benzyl-5-isobutyl-4H-1,2,4-triazol-3-yl)thio)methyl)benzamide (**24**). Using compound **m14** as the acid and [1,1'-biphenyl]-4-amine as the amine. Yellow solid, yield 54%. 1H NMR (400 MHz, DMSO- d_6) δ 10.31 (s, 1H), 7.93–7.84 (m, 4H), 7.72–7.64 (m, 4H), 7.50–7.41 (m, 4H), 7.39–7.23 (m, 4H), 6.98–6.91 (m, 2H), 5.06 (s, 2H), 4.39 (s, 2H), 2.48 (d, $J = 7.2$ Hz, 2H), 1.95–1.81 (m, 1H), 0.84 (d, $J = 6.6$ Hz, 6H). ^{13}C NMR (126 MHz, DMSO) δ 165.58, 155.68, 148.84, 141.59, 140.15, 139.09, 136.18, 135.75, 134.32, 129.38, 129.25, 128.28, 127.54, 127.26, 126.80, 126.75, 121.11, 46.61, 37.36, 33.62, 26.98, 22.57. HPLC $t_R = 3.79$ min, purity:

98.37%. MS (ESI): m/z 533 [M+H]⁺. HRMS (ESI+) calcd for C₃₃H₃₃N₄O₅ [M+H] 533.2370, found 533.2371.

4-(((4-benzyl-5-isobutyl-4H-1,2,4-triazol-3-yl)thio)methyl)-N-(4-methoxyphenyl)benzamide (**25**). Using compound **m14** as the acid and 4-methoxyaniline as the amine. Brown oil, yield 67%. ¹H NMR (400 MHz, DMSO-*d*₆) δ 10.09 (s, 1H), 7.86 (d, *J* = 8.2 Hz, 2H), 7.66 (d, *J* = 9.0 Hz, 2H), 7.41 (d, *J* = 8.2 Hz, 2H), 7.36–7.23 (m, 3H), 6.98–6.88 (m, 4H), 5.05 (s, 2H), 4.38 (s, 2H), 3.74 (s, 3H), 2.47 (d, *J* = 7.2 Hz, 2H), 1.94–1.80 (m, 1H), 0.83 (d, *J* = 6.6 Hz, 6H). ¹³C NMR (126 MHz, DMSO) δ 165.08, 156.02, 155.66, 148.84, 141.30, 136.19, 134.46, 132.64, 129.30, 129.24, 128.24, 128.14, 126.80, 122.44, 114.20, 55.65, 46.61, 37.41, 33.64, 26.98, 22.56. HPLC *t*_R = 3.241 min, purity: 97.08%. MS (ESI): m/z 487 [M+H]⁺. HRMS (ESI+) calcd for C₂₈H₃₁N₄O₂S [M+H] 487.2162, found 487.2169.

4-(((4-benzyl-5-isobutyl-4H-1,2,4-triazol-3-yl)thio)methyl)-N-(2-fluorophenyl)benzamide (**26**). Using compound **m14** as the acid and 2-fluoroaniline as the amine. Pale yellow thick oil, yield 64%. ¹H NMR (400 MHz, DMSO-*d*₆) δ 10.08 (s, 1H), 7.89 (d, *J* = 8.3 Hz, 2H), 7.63–7.54 (m, 1H), 7.42 (d, *J* = 8.2 Hz, 2H), 7.36–7.18 (m, 6H), 6.96–6.89 (m, 2H), 5.05 (s, 2H), 4.39 (s, 2H), 2.47 (d, *J* = 7.2 Hz, 2H), 1.93–1.79 (m, 1H), 0.83 (d, *J* = 6.6 Hz, 6H). ¹³C NMR (126 MHz, DMSO) δ 165.41, 157.27, 155.66, 155.31, 148.80, 141.85, 136.17, 133.33, 129.41, 129.23, 128.36, 128.23, 127.66, 126.79, 124.76, 124.73, 116.36, 116.20, 49.07, 46.62, 37.41, 33.63, 26.98, 22.55. HPLC *t*_R = 3.44 min, purity: 99.13%. MS (ESI): m/z 475 [M+H]⁺.

4-(((4-benzyl-5-isobutyl-4H-1,2,4-triazol-3-yl)thio)methyl)-N-(3-fluorophenyl)benzamide (**27**). Using compound **m14** as the acid and 3-fluoroaniline as the amine. Pale yellow thick oil, yield 65%. ¹H NMR (400 MHz, DMSO-*d*₆) δ 10.39 (s, 1H), 7.87 (d, *J* = 8.3 Hz, 2H), 7.75 (dt, *J* = 11.9, 2.3 Hz, 1H), 7.60–7.52 (m, 1H), 7.47–7.26 (m, 7H), 6.97–6.92 (m, 2H), 5.06 (s, 2H), 4.39 (s, 2H), 2.48 (d, *J* = 7.1 Hz, 2H), 1.93–1.79 (m, 1H), 0.83 (d, *J* = 6.6 Hz, 7H). HPLC *t*_R = 3.61 min, purity: 98.57%. MS (ESI): m/z 475 [M+H]⁺.

4-(((4-benzyl-5-isobutyl-4H-1,2,4-triazol-3-yl)thio)methyl)-N-(4-(trifluoromethyl)phenyl)benzamide (**28**). Using compound **m14** as the acid and 4-(trifluoromethyl)aniline as the amine. Yellow solid, yield 60%. ¹H NMR (400 MHz, DMSO-*d*₆) δ 10.54 (s, 1H), 8.01 (d, *J* = 8.4 Hz, 2H), 7.89 (d, *J* = 8.2 Hz, 2H), 7.73 (d, *J* = 8.5 Hz, 2H), 7.45 (d, *J* = 8.3 Hz, 2H), 7.36–7.23 (m, 3H), 6.98–6.91 (m, 2H), 5.06 (s, 2H), 4.39 (s, 2H), 2.48 (d, *J* = 7.2 Hz, 2H), 1.93–1.81 (m, 1H), 0.83 (d, *J* = 6.6 Hz, 6H). HPLC *t*_R = 3.88 min, purity: 98.39%. MS (ESI): m/z 525 [M+H]⁺.

4-(((4-benzyl-5-isobutyl-4H-1,2,4-triazol-3-yl)thio)methyl)-N-(3-(trifluoromethyl)phenyl)benzamide (**29**). Using compound **m14** as the acid and 3-(trifluoromethyl)aniline as the amine. White wax, yield 68%. ¹H NMR (400 MHz, DMSO-*d*₆) δ 10.52 (s, 1H), 8.25 (s, 1H), 8.05 (d, *J* = 7.6 Hz, 1H), 7.90 (d, *J* = 8.3 Hz, 2H), 7.65–7.56 (m, 1H), 7.49–7.42 (m, 3H), 7.36–7.23 (m, 3H), 6.98–6.91 (m, 2H), 5.06 (s, 2H), 4.39 (s, 2H), 2.48 (d, *J* = 7.2 Hz, 2H), 1.93–1.80 (m, 1H), 0.83 (d, *J* = 6.6 Hz, 6H). ¹³C NMR (126 MHz, DMSO) δ 165.95, 155.68, 148.81, 141.94, 140.40, 136.18, 133.82, 130.33, 129.43, 129.24, 128.33, 128.25, 126.80, 124.23, 116.78, 46.61, 37.32, 33.63, 26.98, 22.56. HPLC *t*_R = 3.63 min, purity: 100%. MS (ESI): m/z 525 [M+H]⁺.

4-(((4-benzyl-5-isobutyl-4H-1,2,4-triazol-3-yl)thio)methyl)-N-(quinolin-6-yl)benzamide (**30**). Using compound **m14** as the acid and quinolin-6-amine as the amine. Brown solid, yield 58%. ¹H NMR (400 MHz, DMSO-*d*₆) δ 10.54 (s, 1H), 8.81 (dd, *J* = 4.2, 1.7 Hz, 1H), 8.55 (d, *J* = 2.1 Hz, 1H), 8.33 (dd, *J* = 8.4, 1.6 Hz, 1H), 8.07–7.99 (m, 2H), 7.94 (d, *J* = 8.2 Hz, 2H), 7.51 (dd, *J* = 8.3, 4.2 Hz, 1H), 7.47 (d, *J* = 8.3 Hz, 2H), 7.37–7.24 (m, 3H), 6.99–6.91 (m, 2H), 5.07 (s, 2H), 4.40 (s, 2H), 2.48 (d, *J* = 7.1 Hz, 2H), 1.95–1.82 (m, 1H), 0.84 (d, *J* = 6.6 Hz, 6H). HPLC *t*_R = 2.88 min, purity: 100%. MS (ESI): m/z 508 [M+H]⁺.

4-(((4-benzyl-5-isobutyl-4H-1,2,4-triazol-3-yl)thio)methyl)-N-cyclohexylbenzamide (**31**). Using compound **m14** as the acid and

cyclohexanamine as the amine. White wax, yield 62%. ¹H NMR (400 MHz, DMSO-*d*₆) δ 8.15 (d, *J* = 8.0 Hz, 1H), 7.74 (d, *J* = 8.2 Hz, 2H), 7.36–7.22 (m, 5H), 6.94–6.87 (m, 2H), 5.03 (s, 2H), 4.34 (s, 2H), 3.79–3.71 (m, 1H), 2.45 (d, *J* = 7.2 Hz, 2H), 1.93–1.77 (m, 3H), 1.76–1.69 (m, 2H), 1.65–1.56 (m, 1H), 1.37–1.26 (m, 4H), 1.20–1.06 (m, 1H), 0.82 (d, *J* = 6.6 Hz, 6H). ¹³C NMR (126 MHz, DMSO) δ 165.31, 155.61, 148.82, 140.73, 136.18, 134.32, 129.21, 129.07, 128.20, 127.88, 126.78, 48.79, 46.60, 37.49, 33.63, 32.86, 26.96, 25.73, 25.43, 22.55. HPLC *t*_R = 3.38 min, purity: 100%. MS (ESI): m/z 463 [M+H]⁺. HRMS (ESI+) calcd for C₂₇H₃₅N₄O₅ [M+H] 463.2526, found 463.2535.

4-(((4-benzyl-5-isobutyl-4H-1,2,4-triazol-3-yl)thio)methyl)-N-(pyridin-3-yl)benzamide (**32**). Using compound **m14** as the acid and pyridin-3-amine as the amine. Yellow solid, 56%. ¹H NMR (400 MHz, DMSO-*d*₆) δ 10.45 (s, 1H), 8.93 (d, *J* = 2.5 Hz, 1H), 8.31 (dd, *J* = 4.6, 1.5 Hz, 1H), 8.19 (d, *J* = 8.5 Hz, 1H), 7.91 (d, *J* = 8.0 Hz, 2H), 7.45 (d, *J* = 8.2 Hz, 2H), 7.40 (dd, *J* = 8.3, 4.7 Hz, 1H), 7.36–7.24 (m, 3H), 6.94 (d, *J* = 6.4 Hz, 2H), 5.06 (s, 2H), 4.39 (s, 2H), 2.48 (d, *J* = 7.2 Hz, 2H), 1.93–1.81 (m, 1H), 0.83 (d, *J* = 6.6 Hz, 6H). HPLC *t*_R = 2.71 min, purity: 98.54%. MS (ESI): m/z 458 [M+H]⁺.

Methyl 4-((2-(trimethylsilyl)ethoxy)methoxy)benzoate (**m16**). Methyl 4-hydroxybenzoate (2.28 g, 15 mmol) and 2-(trimethylsilyl)ethoxymethyl chloride (3.89 mL, 22 mmol) were dissolved in acetonitrile (45 mL), to which cesium carbonate (7.16 g, 22 mol) was added. The mixture was stirred at room temperature overnight. The solvent was removed and the residue was dissolved in ethyl acetate. The organic layer was washed with water and brine, dried with Na₂SO₄, concentrated and purified with sil gel chromatography (5% ethyl acetate in petroleum ether) to get the product as colorless oil (3.26 g, yield 77%). ¹H NMR (400 MHz, Chloroform-*d*) δ 8.05–7.94 (m, 2H), 7.11–7.03 (m, 2H), 5.29 (s, 2H), 3.90 (s, 3H), 3.86–3.66 (m, 2H), 1.07–0.74 (m, 2H).0.01 (s, 9H). MS (ESI): m/z 283 [M+H]⁺.

4-Benzyl-3-((4-methoxybenzyl)thio)-5-((2-(trimethylsilyl)ethoxy)methoxy)phenyl)-4H-1,2,4-triazole (**m19**). Compound **m16** (3.26 g, 12 mmol) was dissolved in methanol (15 mL) and added hydrazine hydrate (2.89 g, 90 mmol). The mixture was refluxed overnight and concentrated to dryness to give the intermediate **m17** without further purification. Compound **m17** (1.94 g, 7 mmol) and benzyl isothiocyanate (0.9 mL, 7 mmol) were dissolved in dry ethanol (15 mL). The mixture was added 21% sodium ethoxide in ethanol (5.13 mL, 14 mmol) and refluxed overnight. The solvent was removed. The residue was added ice-cold water and neutralized by 1N HCl. The precipitation was collected, washed with water and dried to get the product **m18** as pale yellow solid (1.48 g, two steps yield 51%). Compound **m18** (1.48 g 4.4 mmol, and 4-methoxybenzyl bromide (0.89 g, 4.4 mmol) were dissolved in acetonitrile (30 mL). Cesium carbonate (1.58 g, 4.84 mmol) was added to the solution. The mixture was stirred at room temperature overnight. Most of the solvent was removed by vacuum. The residue was added water and extracted with ethyl acetate. The organic layer was washed with brine, dried with Na₂SO₄, concentrated and purified with sil gel chromatography (ethyl acetate: petroleum 2:1) to get the product as white solid (1.15 g, yield 49%). ¹H NMR (400 MHz, Chloroform-*d*) δ 7.46–7.38 (m, 2H), 7.33–7.27 (m, 3H), 7.27–7.22 (m, 2H), 7.13–7.04 (m, 2H), 6.96–6.88 (m, 2H), 6.88–6.77 (m, 2H), 5.25 (s, 2H), 5.00 (s, 2H), 4.40 (s, 2H), 3.86–3.67 (m, 5H), 1.07–0.87 (m, 2H), 0.03–0.01 (m, 9H). MS (ESI): m/z 534 [M+H]⁺.

4-(4-Benzyl-5-((4-methoxybenzyl)thio)-4H-1,2,4-triazol-3-yl)phenol (**m20**). Compound **m19** (900 mg, 1.69 mmol) was dissolved in mixed solvent of CH₂Cl₂: EtOH (1:3) 120 mL. HCl in dioxane (12 mL) was added to the solution. The mixture was stirred at room temperature overnight. Most of the solvent was removed by vacuum. The residue was dissolved in ethyl acetate. The organic layer was washed with water, brine, dried with Na₂SO₄, concentrated and purified with sil gel chromatography (CH₂Cl₂: MeOH 30:1) to

get the product as white solid (610 mg, yield 90%). ^1H NMR (400 MHz, Chloroform-*d*) δ 7.46–7.38 (m, 2H), 7.33–7.27 (m, 3H), 7.27–7.22 (m, 2H), 7.13–7.04 (m, 2H), 6.96–6.88 (m, 2H), 6.88–6.77 (m, 2H), 5.25 (s, 2H), 5.00 (s, 2H), 3.89 (s, 3H). MS (ESI): m/z 404 $[\text{M}+\text{H}]^+$.

2-(4-(4-benzyl-5-((4-methoxybenzyl)thio)-4H-1,2,4-triazol-3-yl)phenoxy)acetic acid (**m22**). Compound **m20** (285 mg, 0.71 mmol) and methyl bromoacetate (98 μL , 0.71 mmol) were dissolved in 4 mL *N,N*-dimethylformamide. K_2CO_3 (147 mg, 1.07 mmol) was added to the solution. The mixture was heated to 50 °C and stirred overnight. The mixture was added water and extracted with ethyl acetate. The organic layer was washed with brine, dried with Na_2SO_4 and concentrated to get the crude product **m21** (666 mg). Compound **m21** (666 mg) was dissolved in 7 mL ethanol. The solution was added 1N NaOH (3 mL) and stirred at room temperature overnight. The mixture was diluted with water and added 1N HCl to pH 4. The aqueous phase was extracted with ethyl acetate for three times. The organic layer was combined, washed with brine, dried with Na_2SO_4 , concentrated and purified with sil gel chromatography (CH_2Cl_2 : MeOH 15:1) to get the product as white solid (200 mg, yield 61%). ^1H NMR (400 MHz, Chloroform-*d*) δ 7.46–7.38 (m, 2H), 7.33–7.27 (m, 3H), 7.27–7.22 (m, 2H), 7.13–7.04 (m, 2H), 6.96–6.88 (m, 2H), 6.88–6.77 (m, 2H), 5.10 (s, 2H), 4.86 (s, 2H), 4.57 (s, 2H), 3.89 (s, 3H). MS (ESI): m/z 462 $[\text{M}+\text{H}]^+$.

General procedure C for compounds **33–39**. Compound **m22** (1 eq.), amines (1 eq.), 1-ethyl-3-(3-dimethylaminopropyl)carbodiimide hydrochloride (1.6 eq.) and 1-hydroxybenzotriazole (1.6 eq.) were dissolved in *N,N*-dimethylformamide. *N,N*-Diisopropylethylamine (3.6 eq.) was added to the solution. The mixture was stirred at room temperature overnight. The mixture was added water and extracted with ethyl acetate. The organic layer was washed with brine, dried with Na_2SO_4 , concentrated and purified with sil gel chromatography to get the corresponding product.

2-(4-(4-Benzyl-5-((4-methoxybenzyl)thio)-4H-1,2,4-triazol-3-yl)phenoxy)-*N*-(4-(dimethylamino)phenyl)acetamide (**33**). Using N^1 , N^1 -dimethylbenzene-1,4-diamine as the amine. Pale yellow solid, yield 27%. ^1H NMR (400 MHz, Chloroform-*d*) δ 8.05 (s, 1H), 7.50–7.43 (m, 2H), 7.43–7.36 (m, 2H), 7.30–7.27 (m, 3H), 7.25–7.21 (m, 2H), 7.04–6.96 (m, 2H), 6.92–6.85 (m, 2H), 6.86–6.77 (m, 2H), 6.73–6.69 (m, 2H), 4.98 (s, 2H), 4.61 (s, 2H), 4.39 (s, 2H), 3.78 (s, 3H), 2.93 (s, 6H). ^{13}C NMR (126 MHz, DMSO) δ 165.71, 159.61, 159.17, 155.52, 150.89, 147.83, 136.08, 130.72, 130.20, 129.26, 129.20, 128.43, 128.18, 126.48, 121.68, 120.28, 115.59, 114.35, 112.99, 67.64, 55.57, 47.63, 40.90, 37.34. HPLC t_{R} = 2.85 min, purity: 96.26%. MS (ESI): m/z 580 $[\text{M}+\text{H}]^+$.

2-(4-(4-Benzyl-5-((4-methoxybenzyl)thio)-4H-1,2,4-triazol-3-yl)phenoxy)-*N*-(pyridin-3-yl)acetamide (**34**). Using pyridin-3-amine as the amine. Pale yellow solid, yield 81%. ^1H NMR (400 MHz, Chloroform-*d*) δ 8.87 (s, 1H), 8.72 (d, J = 2.5 Hz, 1H), 8.39 (d, J = 4.7 Hz, 1H), 8.30–8.11 (m, 1H), 7.42 (d, J = 8.4 Hz, 2H), 7.34–7.25 (m, 3H), 7.22 (d, J = 8.3 Hz, 2H), 6.99 (d, J = 8.5 Hz, 2H), 6.93–6.84 (m, 2H), 6.84–6.75 (m, 2H), 4.99 (s, 2H), 4.66 (s, 2H), 4.37 (s, 2H), 3.78 (s, 3H). ^{13}C NMR (126 MHz, DMSO) δ 167.32, 159.48, 159.17, 155.49, 150.91, 145.17, 141.84, 136.07, 135.46, 130.72, 130.24, 129.25, 129.20, 128.17, 127.26, 126.48, 124.09, 120.43, 115.61, 114.35, 67.45, 55.57, 47.64, 37.33. HPLC t_{R} = 2.97 min, purity: 97.78%. MS (ESI): m/z 538 $[\text{M}+\text{H}]^+$.

2-(4-(4-Benzyl-5-((4-methoxybenzyl)thio)-4H-1,2,4-triazol-3-yl)phenoxy)-*N*-(1-methyl-1H-pyrazol-4-yl)acetamide (**35**). Using 1-methyl-1H-pyrazol-4-amine as the amine. Beige solid, yield 55%. ^1H NMR (400 MHz, Chloroform-*d*) δ 8.21 (s, 1H), 7.97 (s, 1H), 7.47 (d, J = 8.2 Hz, 3H), 7.30 (t, J = 3.2 Hz, 2H), 7.24 (s, 2H), 7.01 (d, J = 8.4 Hz, 2H), 6.91 (d, J = 4.5 Hz, 2H), 6.84 (d, J = 8.4 Hz, 2H), 5.01 (s, 2H), 4.64 (s, 2H), 4.41 (s, 2H), 3.91 (s, 3H), 3.81 (s, 3H). ^{13}C NMR (126 MHz,

DMSO) δ 165.02, 159.47, 159.17, 155.49, 150.91, 136.07, 130.72, 130.44, 130.23, 129.26, 129.20, 128.18, 126.48, 122.05, 121.21, 120.41, 115.65, 114.35, 67.49, 55.57, 47.63, 39.12, 37.33. HPLC t_{R} = 3.25 min, purity: 98.57%. MS (ESI): m/z 541 $[\text{M}+\text{H}]^+$.

2-(4-(4-Benzyl-5-((4-methoxybenzyl)thio)-4H-1,2,4-triazol-3-yl)phenoxy)-*N*-(1,3-dimethyl-1H-pyrazol-5-yl)acetamide (**36**). Using 1,3-dimethyl-1H-pyrazol-5-amine as the amine. White solid, yield 76%. ^1H NMR (400 MHz, Chloroform-*d*) δ 8.48 (s, 1H), 7.44 (d, J = 8.6 Hz, 2H), 7.34–7.26 (m, 3H), 7.22 (s, 2H), 6.99 (d, J = 8.5 Hz, 2H), 6.89 (dd, J = 6.8, 2.7 Hz, 2H), 6.82 (d, J = 8.5 Hz, 2H), 6.10 (s, 1H), 5.00 (s, 2H), 4.70 (s, 2H), 4.38 (s, 2H), 3.80 (s, 3H), 3.66 (s, 3H), 2.24 (s, 3H). HPLC t_{R} = 3.23 min, purity: 97.83%. MS (ESI): m/z 555 $[\text{M}+\text{H}]^+$.

2-(4-(4-Benzyl-5-((4-methoxybenzyl)thio)-4H-1,2,4-triazol-3-yl)phenoxy)-*N*-cyclohexylacetamide (**37**). Using cyclohexanamine as the amine. White solid, yield 34%. ^1H NMR (400 MHz, Chloroform-*d*) δ 7.47–7.38 (m, 2H), 7.31–7.25 (m, 3H), 7.24–7.18 (m, 2H), 6.96–6.90 (m, 2H), 6.90–6.84 (m, 2H), 6.84–6.76 (m, 2H), 6.36 (d, J = 8.5 Hz, 1H), 4.97 (s, 2H), 4.46 (s, 2H), 4.38 (s, 2H), 3.91–3.80 (m, 1H), 3.78 (s, 3H), 1.98–1.85 (m, 3H), 1.75–1.67 (m, 2H), 1.44–1.30 (m, 2H), 1.23–1.07 (m, 3H). ^{13}C NMR (126 MHz, DMSO) δ 166.55, 159.54, 159.17, 155.51, 150.86, 136.07, 130.71, 130.16, 129.24, 129.20, 128.18, 126.49, 120.22, 115.57, 114.35, 67.41, 55.57, 47.91, 47.62, 37.34, 32.69, 25.61, 25.09. HPLC t_{R} = 3.54 min, purity: 95.74%. MS (ESI): m/z 543 $[\text{M}+\text{H}]^+$.

2-(4-(4-Benzyl-5-((4-methoxybenzyl)thio)-4H-1,2,4-triazol-3-yl)phenoxy)-*N*-(2-(dimethylamino)ethyl)acetamide (**38**). Using N^1 , N^1 -dimethylethane-1,2-diamine as the amine. White solid, yield 88%. ^1H NMR (400 MHz, Chloroform-*d*) δ 8.03 (s, 1H), 7.47–7.36 (m, 2H), 7.30–7.25 (m, 3H), 7.24–7.20 (m, 2H), 7.06–7.00 (m, 2H), 6.91–6.86 (m, 2H), 6.83–6.79 (m, 2H), 4.98 (s, 2H), 4.55 (s, 2H), 4.37 (s, 2H), 3.79 (s, 3H), 3.66 (q, J = 5.7 Hz, 2H), 2.96 (t, J = 5.7 Hz, 2H), 2.63 (s, 6H). HPLC t_{R} = 2.90 min, purity: 100%. MS (ESI): m/z 532 $[\text{M}+\text{H}]^+$.

2-(4-(4-Benzyl-5-((4-methoxybenzyl)thio)-4H-1,2,4-triazol-3-yl)phenoxy)-*N*-(3-(diethylamino)propyl)acetamide (**39**). Using N^1 , N^1 -diethylpropane-1,3-diamine as the amine. White solid, yield 81%. ^1H NMR (400 MHz, Chloroform-*d*) δ 8.00–7.79 (m, 1H), 7.45–7.38 (m, 2H), 7.31–7.25 (m, 3H), 7.25–7.19 (m, 2H), 7.08–7.00 (m, 2H), 6.88 (ddd, J = 6.0, 3.4, 1.6 Hz, 2H), 6.85–6.76 (m, 2H), 4.98 (s, 2H), 4.54 (s, 2H), 4.38 (s, 2H), 3.79 (s, 3H), 3.50 (dd, J = 11.8, 5.5 Hz, 2H), 3.07 (q, J = 7.3 Hz, 4H), 2.95 (t, J = 7.4 Hz, 2H), 2.13–2.05 (m, 2H), 1.33 (t, J = 7.3 Hz, 6H). HPLC t_{R} = 3.00 min, purity: 100%. MS (ESI): m/z 574 $[\text{M}+\text{H}]^+$.

N-benzyl-3-(4-methoxyphenyl)propanamide (**m24**). 3-(4-Methoxyphenyl)propanoic acid (500 mg, 2.78 mmol), benzylamine (300 mg, 2.78 mmol), 1-ethyl-3-(3-dimethylaminopropyl)carbodiimide hydrochloride (848 mg, 4.44 mmol) and 1-hydroxybenzotriazole (594 mg, 4.44 mmol) were dissolved in 10 mL *N,N*-dimethylformamide. The mixture was added diisopropylethylamine (3 mL, 7.84 mmol) and stirred at room temperature overnight. The mixture was added water and extracted with ethyl acetate. The organic layer was washed with brine, dried with Na_2SO_4 , concentrated and purified with sil gel chromatography (ethyl acetate: petroleum 1:1) to get the product as white solid (650 mg, yield 83%). ^1H NMR (400 MHz, Chloroform-*d*) δ 7.44–7.25 (m, 3H), 7.23–7.06 (m, 4H), 6.98–6.69 (m, 2H), 4.42 (d, J = 5.7 Hz, 2H), 3.81 (s, 3H), 2.96 (t, J = 7.5 Hz, 2H), 2.51 (t, J = 7.5 Hz, 2H). MS (ESI): m/z 270 $[\text{M}+\text{H}]^+$.

N-benzyl-3-(4-methoxyphenyl)propanethioamide (**m25**). Compound **m24** (1.4 g, 5.3 mmol) and Lawesson reagent (1.26 g, 2.7 mmol) were dissolved in 10 mL toluene. The mixture was refluxed for 5 h. The mixture was diluted with ethyl acetate and washed with water. The organic layer was washed with brine, dried with Na_2SO_4 , concentrated and purified with sil gel

chromatography (ethyl acetate: petroleum 4:1) to get the product as pale yellow solid (700 mg, yield 47%). $^1\text{H NMR}$ (400 MHz, Chloroform-*d*) δ 7.44–7.06 (m, 7H), 6.94–6.59 (m, 2H), 4.73 (d, $J = 5.1$ Hz, 2H), 3.80 (s, 3H), 3.10 (t, $J = 7.2$ Hz, 2H), 2.95 (t, $J = 7.2$ Hz, 2H). MS (ESI): m/z 286 $[\text{M}+\text{H}]^+$.

4-Benzyl-3-(4-methoxyphenethyl)-5-(4-((2-(trimethylsilyl)ethoxy)methoxy)phenyl)-4H-1,2,4-triazole (**m26**). Compound **m25** (791 mg, 2.8 mmol) and compound **m17** (1.09 g, 3.5 mmol) were dissolved in dry tetrahydrofuran. The mixture was added HOAc (2.4 mL) and stirred at 0 °C for 10 min. After the addition of HgOAc (800 mg, 3.07 mmol), the mixture stirred at 0 °C for 2 h and overnight at room temperature. The mixture was filtered through diatomite and filtrate was concentrated. The residue was dissolved in ethyl acetate and washed with water. The organic layer was washed with brine, dried with Na_2SO_4 , concentrated and purified with sil gel chromatography (CH_2Cl_2 : MeOH 15:1) to get the product as pale yellow solid (578 mg, yield 55%). $^1\text{H NMR}$ (400 MHz, Chloroform-*d*) δ 7.45–7.39 (m, 2H), 7.38–7.31 (m, 3H), 7.10–7.05 (m, 2H), 7.01 (dd, $J = 8.7, 2.4$ Hz, 2H), 6.91 (dd, $J = 7.3, 2.1$ Hz, 2H), 6.84–6.78 (m, 2H), 5.25 (s, 2H), 4.93 (s, 2H), 3.80 (d, $J = 0.5$ Hz, 3H), 3.78–3.73 (m, 2H), 3.03 (dd, $J = 9.3, 6.4$ Hz, 2H), 2.86 (dd, $J = 9.0, 6.6$ Hz, 2H), 0.98–0.92 (m, 2H), 0.02–0.00 (s, 9H). MS (ESI): m/z 516 $[\text{M}+\text{H}]^+$.

Methyl 2-(4-(4-benzyl-5-(4-methoxyphenethyl)-4H-1,2,4-triazol-3-yl)phenoxy)acetate (**m28**). Compound **m26** (378 mg, 0.73 mmol) was dissolved in mixed solvent of CH_2Cl_2 : EtOH (1:3) 12 mL. HCl in dioxane (3 mL) was added to the solution. The mixture was stirred at room temperature overnight. Most of the solvent was removed by vacuum. The residue was dissolved in ethyl acetate. The organic layer was washed with water, brine, dried with Na_2SO_4 , concentrated and purified with sil gel chromatography (CH_2Cl_2 : MeOH 30:1) to get the product **m27** as white solid (271 mg, yield 96%). Compound **m27** (271 mg, 0.7 mmol) and methyl bromoacetate (66 μL , 0.7 mmol) were dissolved in 4 mL *N,N*-dimethylformamide. K_2CO_3 (193 mg, 2.5 mmol) was added to the solution. The mixture was heated to 50 °C and stirred overnight. The mixture was added water and extracted with ethyl acetate. The organic layer was washed with brine, dried with Na_2SO_4 , concentrated and purified with sil gel chromatography (ethyl acetate: petroleum 2:1) to get the product as pale yellow oil (304 mg, 95%). $^1\text{H NMR}$ (400 MHz, DMSO-*d*₆) δ 7.61–7.54 (m, 2H), 7.33–7.30 (m, 3H), 7.11–7.06 (m, 2H), 7.03–6.98 (m, 2H), 6.92 (d, $J = 7.3$ Hz, 2H), 6.85–6.80 (m, 2H), 5.23 (s, 2H), 4.72 (s, 2H), 3.82 (s, 3H), 3.71 (s, 3H), 2.88 (d, $J = 6.4$ Hz, 2H), 2.86–2.81 (m, 2H). MS (ESI): m/z 458 $[\text{M}+\text{H}]^+$.

Methyl 2-(4-(4-benzyl-5-(4-methoxyphenethyl)-4H-1,2,4-triazol-3-yl)phenoxy)propanoate (**m29**). The same method as compound **m28**, using methyl 2-bromopropanoate to replace methyl bromoacetate. White solid, yield 75%. $^1\text{H NMR}$ (400 MHz, Chloroform-*d*) δ 7.47–7.38 (m, 2H), 7.37–7.29 (m, 3H), 7.06–6.97 (m, 2H), 6.90–6.86 (m, 4H), 6.82–6.76 (m, 2H), 4.92 (s, 2H), 4.78 (q, $J = 6.8$ Hz, 1H), 3.78 (s, 3H), 3.75 (s, 3H), 3.07–3.00 (m, 2H), 2.87–2.80 (m, 2H), 1.63 (d, $J = 6.8$ Hz, 3H). MS (ESI): m/z 472 $[\text{M}+\text{H}]^+$.

Methyl 2-(4-(4-benzyl-5-(4-methoxyphenethyl)-4H-1,2,4-triazol-3-yl)phenoxy)butanoate (**m30**). The same method as compound **m28**, using methyl 2-bromobutanoate to replace methyl bromoacetate. White solid, yield 76%. $^1\text{H NMR}$ (400 MHz, Chloroform-*d*) δ 7.47–7.38 (m, 2H), 7.39–7.30 (m, 3H), 7.06–6.97 (m, 2H), 6.94–6.86 (m, 4H), 6.85–6.76 (m, 2H), 4.92 (s, 2H), 4.60 (t, $J = 6.2$ Hz, 1H), 3.78 (s, 3H), 3.75 (s, 3H), 3.08–3.00 (m, 2H), 2.88–2.81 (m, 2H), 2.05–1.96 (m, 2H), 1.07 (t, $J = 7.4$ Hz, 3H). MS (ESI): m/z 486 $[\text{M}+\text{H}]^+$.

Methyl 2-(4-(4-benzyl-5-(4-methoxyphenethyl)-4H-1,2,4-triazol-3-yl)phenoxy)-2-methylpropanoate (**m31**). The same

method as compound **m28**, using methyl 2-bromo-2-methylpropanoate to replace methyl bromoacetate. White solid, yield 72%. $^1\text{H NMR}$ (400 MHz, Chloroform-*d*) δ 7.39–7.32 (m, 2H), 7.30–7.22 (m, 3H), 7.00–6.91 (m, 2H), 6.84 (dd, $J = 7.3, 2.2$ Hz, 2H), 6.81–6.70 (m, 4H), 4.90 (s, 2H), 3.70 (d, $J = 5.4$ Hz, 6H), 3.01–2.94 (m, 2H), 2.84–2.76 (m, 2H), 1.56 (s, 6H). MS (ESI): m/z 486 $[\text{M}+\text{H}]^+$.

General procedure D for compounds **40–43**. Compounds **m28–31** (1 eq.) were dissolved in EtOH. 1N NaOH (5 eq.) was added to the solution (1N NaOH/EtOH v/v: 1/2). The mixture was stirred at room temperature overnight. The mixture was diluted with water and added 1N HCl to pH 4. The precipitation was filtered, washed with water and dried to get intermediate products **m32–35**. Compounds **m32–35** were dissolved in DMF. 1-Methyl-1H-pyrazol-4-amine (1 eq.), 1-hydroxybenzotriazole (1.5 eq.), 1-ethyl-3-(3-dimethylaminopropyl)carbodiimide hydrochloride (1.5 eq.), and *N,N*-diisopropylethylamine (3.5 eq.) were added to solution. The mixture was stirred at room temperature overnight. The mixture was diluted with water and extracted with ethyl acetate. The organic layer was washed with brine, dried with Na_2SO_4 , concentrated and purified with sil gel chromatography (CH_2Cl_2 : MeOH 30:1) to get the product **40–43**.

2-(4-(4-Benzyl-5-(4-methoxyphenethyl)-4H-1,2,4-triazol-3-yl)phenoxy)-*N*-(1-methyl-1H-pyrazol-4-yl)acetamide (**40**). White solid, yield of two steps 53%. $^1\text{H NMR}$ (400 MHz, Chloroform-*d*) δ 8.28 (s, 1H), 7.97 (s, 1H), 7.54–7.44 (m, 3H), 7.38–7.30 (m, 3H), 7.09–6.96 (m, 5H), 6.95–6.87 (m, 2H), 6.82 (d, $J = 8.6$ Hz, 2H), 4.94 (s, 2H), 4.64 (s, 2H), 3.90 (s, 3H), 3.80 (s, 3H), 3.07 (t, 2H), 2.89 (t, 2H). HPLC $t_R = 3.02$ min, purity: 100%. MS (ESI): m/z 523 $[\text{M}+\text{H}]^+$.

2-(4-(4-Benzyl-5-(4-methoxyphenethyl)-4H-1,2,4-triazol-3-yl)phenoxy)-*N*-(1-methyl-1H-pyrazol-4-yl)propanamide (**41**). White solid, yield of two steps 26%. $^1\text{H NMR}$ (400 MHz, Chloroform-*d*) δ 8.19 (s, 1H), 7.92 (s, 1H), 7.49–7.43 (m, 2H), 7.40 (s, 1H), 7.38–7.27 (m, 3H), 7.04–6.99 (m, 2H), 6.99–6.94 (m, 2H), 6.88 (dd, $J = 7.2, 2.4$ Hz, 2H), 6.84–6.75 (m, 2H), 4.91 (s, 2H), 4.80 (q, $J = 6.7$ Hz, 1H), 3.86 (s, 3H), 3.77 (s, 3H), 3.04 (t, $J = 7.8$ Hz, 2H), 2.86 (t, $J = 9.3, 6.3$ Hz, 2H), 1.63 (d, $J = 6.7$ Hz, 3H). $^{13}\text{C NMR}$ (126 MHz, DMSO) δ 168.46, 158.75, 158.12, 155.01, 154.21, 136.61, 133.06, 130.37, 129.76, 129.36, 128.10, 126.30, 122.00, 121.31, 120.89, 115.99, 114.18, 74.24, 55.46, 46.74, 39.09, 32.02, 27.26, 19.05. HPLC $t_R = 2.85$ min, purity: 100%. MS (ESI): m/z 537 $[\text{M}+\text{H}]^+$.

2-(4-(4-Benzyl-5-(4-methoxyphenethyl)-4H-1,2,4-triazol-3-yl)phenoxy)-*N*-(1-methyl-1H-pyrazol-4-yl)butanamide (**42**). White solid, yield of two steps 33%. $^1\text{H NMR}$ (400 MHz, Chloroform-*d*) δ 8.50 (s, 1H), 7.91 (s, 1H), 7.44–7.36 (m, 3H), 7.36–7.28 (m, 3H), 7.04–6.97 (m, 2H), 6.97–6.90 (m, 2H), 6.90–6.84 (m, 2H), 6.82–6.74 (m, 2H), 4.90 (s, 2H), 4.62 (t, $J = 6.5, 4.9$ Hz, 1H), 3.83 (s, 3H), 3.76 (s, 3H), 3.01 (t, $J = 9.1, 6.5$ Hz, 2H), 2.84 (t, $J = 8.9, 6.7$ Hz, 2H), 2.09–1.93 (m, 2H), 1.02 (t, $J = 7.4$ Hz, 3H). HPLC $t_R = 2.93$ min, purity: 100%. MS (ESI): m/z 551 $[\text{M}+\text{H}]^+$.

2-(4-(4-Benzyl-5-(4-methoxyphenethyl)-4H-1,2,4-triazol-3-yl)phenoxy)-2-methyl-*N*-(1-methyl-1H-pyrazol-4-yl)propanamide (**43**). White solid, yield of two steps 28%. $^1\text{H NMR}$ (400 MHz, Chloroform-*d*) δ 8.67 (s, 1H), 7.92 (s, 1H), 7.44–7.36 (m, 3H), 7.36–7.27 (m, 3H), 7.02–6.96 (m, 2H), 6.95–6.89 (m, 2H), 6.89–6.84 (m, 2H), 6.82–6.74 (m, 2H), 4.91 (s, 2H), 3.84 (s, 3H), 3.75 (s, 3H), 3.01 (t, $J = 7.8$ Hz, 2H), 2.84 (t, $J = 9.3, 6.3$ Hz, 2H), 1.56 (s, 6H). $^{13}\text{C NMR}$ (126 MHz, DMSO) δ 170.94, 158.13, 156.48, 155.04, 154.12, 136.56, 133.05, 130.63, 130.09, 129.77, 129.31, 128.09, 126.43, 121.96, 121.82, 121.73, 120.08, 114.18, 81.02, 55.46, 46.79, 39.10, 32.04, 27.25, 25.40. HPLC $t_R = 2.94$ min, purity: 100%. MS (ESI): m/z 551 $[\text{M}+\text{H}]^+$.

Protein expression The PDE δ protein sequence was cloned into PET28 vector with His-tag in the N-terminal. Colonies from freshly transformed plasmid DNA in *E. coli* BL21(DE3)-condon plus-RIL cells, were grown overnight at 37 °C in 50 mL of Terrific Broth

medium with 50 µg/mL kanamycin and 34 µg/mL chloramphenicol (start-up culture). Then start-up culture was diluted 100 fold in 1 L fresh TB medium and cell was growth at 37 °C to an optical density of about 0.8 at OD600 before the temperature was decreased to 16 °C. When the system equilibrated at 16 °C the optical density was about 1.2 at OD600 and protein expression was induced overnight at 16 °C with 0.2 mM isopropyl-β-Dthiogalactopyranoside (IPTG). The bacteria were harvested by centrifugation (4000×g for 20 min at 4 °C) and were frozen at –80 °C as pellets for storage. Cells expressing His6-tagged proteins were re-suspended in lysis buffer (50 mM Tris, pH 8.0 at 4 °C, 250 mM NaCl, 5 mM Imidazole, 5% glycerol with freshly added 0.5 mM TCEP (Tris(2-carboxyethyl) phosphine hydrochloride) and 1 mM PMSF(Phenylmethanesulfonyl fluoride)) and lysed using an UN-03 high pressure homogenizer (Union-biotech – Shanghai, China) at 4 °C. The lysate was cleared by centrifugation (12,000×g for 1 h at 4 °C) and was applied to a Ni-Sepharose6-fast-flow column. The column was washed twice with 50 mL of wash buffer containing 30 mM Imidazole. The protein was eluted using a step elution of imidazole in elution buffer (80, 250 mM Imidazole in 50 mM Tris, pH 8.0 at 4 °C, 250 mM NaCl, 5% glycerol). All fractions were collected and monitored by SDS-polyacrylamide gel electrophoresis (Bio-Rad Criterion™ Precast Gels, 4–12% Bis-Tris, 1.0 mm, from Bio-Rad, CA.). After the addition of 1 mM dithiothreitol (DTT), the eluted protein was treated overnight at 4 °C with Tobacco Etch Virus (TEV) protease to remove the His6 tag. The protein was concentrated and further purified with size exclusion chromatography on a Superdex 75 16/60 HiLoad gel filtration column. Samples were monitored by SDS-polyacrylamide gel electrophoresis and concentrated to 8–10 mg/mL in the gel filtration buffer, 10 mM Tris pH 8.0, 250 mM NaCl, 1 mM DTT and were used for ibinding assay and crystallization.

Crystallization and X-ray Crystallography Aliquots of the purified proteins were set up for crystallization using the vapour diffusion method. PDEδ and inhibitors were co-crystallized by mixing a solution of 1 mM small molecule and 500 µM PDEδ with 1%DMSO as a final concentration. Crystals were obtained in condition containing 100 mM sodium acetate PH4.6 and 3.0 M NaCl. The crystals were flash frozen in a buffer that contained the mother liquor components in addition to 30% glycerol as a cryoprotectant. Data were collected at 100 K on beamline BL17U at the Shanghai Synchrotron Radiation Facility (SSRF) (Shanghai, China) for the co-crystallized structures [27]. The data were processed with the HKL2000 software packages [28], and the structures were then solved by molecular replacement, using the CCP4 program MOLREP [29]. The search model used for the crystals was the PDEδ-farnesylated Rheb complex structure (PDB code 3T5G). The structures were refined using the CCP4 program REFMAC5 [30] combined with the simulated-annealing protocol implemented in the program PHENIX [31]. With the aid of the program Coot [32], compound, water molecules, and others were fitted into to the initial Fo-Fc maps. The complete statistics, as well as the quality of the solved structure, are shown in Table S1.

Hit compound screening. The fragment compound library set-up previously was used in the PDEδ-targeted hit compound screening. And two cycles of ligand observed T1ρ and saturation transfer difference (STD) NMR experiments were carried out to identify the hit compounds. The mixed samples of either 200 µM group fragments or 200 µM single compound and 5 µM PDEδ protein, were dissolved in phosphate buffer (20 mM NaH₂PO₄/Na₂HPO₄, 100 mM NaCl, 2% DMSO, at pH 7.4) and used in NMR data acquisition. All of the NMR experiments were acquired at 25 °C on Bruker Avance III 600 MHz NMR spectrometer equipped with a cryogenically cooled probe (The NMR spectra were shown in Figs. S2–S6.).

Fluorescence anisotropy assay. The binding of compounds to

PDEδ was assessed using a Fluorescence Anisotropy Binding Assay. The fluorescent ligand was prepared by attaching a fluorescent fragment (Fluorescein IsoThioCyanate isomer I, 5-FITC, CAS number: 3326-32-7) to the Atorvastatin. Generally, the method involves incubating the protein PDEδ, fluorescent ligand and a variable concentration of test compound. Detailedly, all components were dissolved in buffer of PBS adding 0.5 mM CHAPS with final concentrations of PDEδ 20 nM, fluorescent ligand 25 nM. This reaction mixture was added various concentrations of test compound or DMSO vehicle (2% final) in Corning 384 well Black low volume plate (CLS3575) and equilibrated in dark 4 h at room temperature. Fluorescence anisotropy was read on BioTek Synergy2 Multi-Mode Microplate Reader (ex = 485 nm, EM = 530 nm; Dichroic –505 nm).

Cell lines and culture conditions. Human non-small cell lung cancer cell line A549 and H460 were purchased from American Type Culture Collection (ATCC). A549 cells were cultured in Ham's F-12 medium supplemented with 10% fetal bovine serum, and H460 cell were cultured in RPMI 1640 supplemented with 10% fetal bovine serum. Cells were maintained in a humidified incubator with 5% CO₂ at 37 °C.

Cell viability assay. Cells were seeded in 96-well plates overnight and treated with the indicated drugs. Sulforhodamine B assay (SRB, Sigma) was performed after incubation for 72 h. IC₅₀ values were calculated by concentration-response curve fitting using four-parameter method.

Western blots. Cells were lysed with 2% Sodium laurylsulfonate (SDS), boiled in a 100° metallic bath for 30 min, and quantified by Bicinchoninic acid (BCA, Beyotime). SDS-polyacrylamide gel electrophoresis was carried out with 10–25 µg of whole-cell lysate from each sample. The gels were blotted onto nitrocellulose membrane and blocked for 1.5 h at room temperature. Antibodies used for western blotting included: Phospho-c-Raf-Ser338 (Cell Signaling, #9427), c-Raf (Cell Signaling, #53745S), Phospho-Erk1/2-Thr202/Tyr204 (Cell Signaling, #4370), Erk1/2 (Cell Signaling, #4695), Phospho-p70 S6-Thr389 (Cell Signaling, #9234), p70 S6 Kinase (Cell Signaling, #2708S) and GAPDH (Proteintech).

Author contributions

The manuscript was written through contributions of all authors. All authors have given approval to the final version of the manuscript.

Funding sources

Financial supported by the National Natural Science Foundation of China (Grant No. 81330076, 81473094, 81402850), the “Personalized Medicines Molecular Signature-based Drug Discovery and Development”, Strategic Priority Research Program of the Chinese Academy of Sciences (Grant No. XDA12020345). And the Institutes for Drug Discovery and Development, Chinese Academy of Sciences (No. CASIMM0120164002 and CASIMM0120163013).

Acknowledgment

We thank the staff at beamline BL-17U of Shanghai Light Source for supporting the X-ray data collection. This research has been financially supported by grants from the Strategic Priority Research Program of the Chinese Academy of Sciences (No. XDA12020345 to Xin Wang), National Natural Science Foundation of China (Grant No. 81473094 and 81402850 to Bing Xiong and Jian Li) and the Institutes for Drug Discovery and Development, Chinese Academy of Sciences (No. CASIMM0120164002 and CASIMM0120163013 to Naixia Zhang).

Appendix A. Supplementary data

Supplementary data to this article can be found online at <https://doi.org/10.1016/j.ejmech.2018.12.018>.

References

- [1] D.K. Simanshu, D.V. Nissley, F. McCormick, RAS proteins and their regulators in human disease, *Cell* 170 (2017) 17–33.
- [2] A.D. Cox, C.J. Der, Ras history: the saga continues, *Small GTPases* 1 (2010) 2–7.
- [3] A.D. Cox, S.W. Fesik, A.C. Kimmelman, J. Luo, C.J. Der, Drugging the undruggable RAS: mission possible? *Nat. Rev. Drug Discov.* 13 (2014) 828–851.
- [4] B. Papke, C.J. Der, Drugging RAS: Know the Enemy, vol. 355, 2017, pp. 1158–1163.
- [5] Z. Tan, S. Zhang, Past, present, and future of targeting Ras for cancer therapies, *Mini Rev. Med. Chem.* 16 (2016) 345–357.
- [6] J.M. Ostrem, K.M. Shokat, Direct small-molecule inhibitors of KRAS: from structural insights to mechanism-based design, *Nat. Rev. Drug Discov.* 15 (2016) 771–785.
- [7] J. Spiegel, P.M. Cromm, G. Zimmermann, T.N. Grossmann, H. Waldmann, Small-molecule modulation of Ras signaling, *Nat. Chem. Biol.* 10 (2014) 613–622.
- [8] J.P. O'Bryan, Pharmacological Targeting of RAS: Recent Success with Direct Inhibitors, *Pharmacological research*, 2018.
- [9] C.E. Quevedo, A. Cruz-Migoni, Small Molecule Inhibitors of RAS-Effector Protein Interactions Derived Using an Intracellular Antibody Fragment, vol. 9, 2018, p. 3169.
- [10] A.B. Keeton, E.A. Salter, G.A. Piazza, The RAS-effector interaction as a drug target, *Cancer Res.* 77 (2017) 221–226.
- [11] S. Lu, H. Jang, J. Zhang, R. Nussinov, Inhibitors of ras-SOS interactions, *ChemMedChem* 11 (2016) 814–821.
- [12] B. Frett, Y. Wang, H.Y. Li, Targeting the K-Ras/PDEdelta protein-protein interaction: the solution for Ras-driven cancers or just another therapeutic mirage? *ChemMedChem* 8 (2013) 1620–1622.
- [13] D.T.S. Lin, N.G. Davis, E. Conibear, Targeting the Ras Palmitoylation/depalmitoylation Cycle in Cancer, *Biochemical Society transactions*, 2017.
- [14] B. Sautier, C.F. Nising, L. Wortmann, Latest advances towards Ras inhibition: a medicinal chemistry perspective, *Angew. Chem.* 55 (2016) 15982–15988.
- [15] V. Nancy, I. Callebaut, A. El Marjou, J. de Gunzburg, The delta subunit of retinal rod cGMP phosphodiesterase regulates the membrane association of Ras and Rap GTPases, *J. Biol. Chem.* 277 (2002) 15076–15084.
- [16] G. Zimmermann, B. Papke, S. Ismail, N. Vartak, A. Chandra, M. Hoffmann, S.A. Hahn, G. Triola, A. Wittinghofer, P.I. Bastiaens, H. Waldmann, Small molecule inhibition of the KRAS-PDEdelta interaction impairs oncogenic KRAS signalling, *Nature* 497 (2013) 638–642.
- [17] L. Zhao, D. Cao, T. Chen, Y. Wang, Z. Miao, Y. Xu, W. Chen, X. Wang, Y. Li, Z. Du, B. Xiong, J. Li, C. Xu, N. Zhang, J. He, J. Shen, Fragment-based drug discovery of 2-thiazolidinones as inhibitors of the histone reader BRD4 bromodomain, *J. Med. Chem.* 56 (2013) 3833–3851.
- [18] J.L. Yu, T.T. Chen, C. Zhou, F.L. Lian, X.L. Tang, Y. Wen, J.K. Shen, Y.C. Xu, B. Xiong, N.X. Zhang, NMR-based platform for fragment-based lead discovery used in screening BRD4-targeted compounds, *Acta Pharmacol. Sin.* 37 (2016) 984–993.
- [19] B. Papke, S. Murarka, H.A. Vogel, P. Martin-Gago, M. Kovacevic, D.C. Truxius, E.K. Fansa, S. Ismail, G. Zimmermann, K. Heinelt, C. Schultz-Fademrecht, A. Al Saabi, M. Baumann, P. Nussbaumer, Identification of Pyrazolopyridazinones as PDEdelta Inhibitors, vol. 7, 2016, p. 11360.
- [20] P. Martin-Gago, E.K. Fansa, C.H. Klein, S. Murarka, P. Janning, M. Schurmann, M. Metz, S. Ismail, C. Schultz-Fademrecht, M. Baumann, P.I. Bastiaens, A. Wittinghofer, H. Waldmann, A PDEdelta-KRas inhibitor chemotype with up to seven H-bonds and picomolar affinity that prevents efficient inhibitor release by Arl2, *Angew. Chem.* 56 (2017) 2423–2428.
- [21] L. Chen, C. Zhuang, J. Lu, Y. Jiang, C. Sheng, Discovery of novel KRAS-PDEdelta inhibitors by fragment-based drug design, *J. Med. Chem.* 61 (2018) 2604–2610.
- [22] Y. Jiang, C. Zhuang, L. Chen, J. Lu, G. Dong, Z. Miao, W. Zhang, J. Li, C. Sheng, Structural biology-inspired discovery of novel KRAS-PDEdelta inhibitors, *J. Med. Chem.* 60 (2017) 9400–9406.
- [23] D.E. Scott, A.G. Coyne, S.A. Hudson, C. Abell, Fragment-based approaches in drug discovery and chemical biology, *Biochemistry* 51 (2012) 4990–5003.
- [24] M. Hanzal-Bayer, L. Renault, P. Roversi, A. Wittinghofer, R.C. Hillig, The complex of Arl2-GTP and PDE delta: from structure to function, *EMBO J.* 21 (2002) 2095–2106.
- [25] S. Dharmiaiah, L. Bindu, T.H. Tran, W.K. Gillette, P.H. Frank, R. Ghirlando, D.V. Nissley, D. Esposito, F. McCormick, A.G. Ctephen, D.K. Simanshu, Structural basis of recognition of farnesylated and methylated KRAS4b by PDEdelta, *Proc. Natl. Acad. Sci. U. S. A.* 113 (2016) E6766–E6775.
- [26] A. Chandra, H.E. Grecco, V. Pisupati, D. Perera, L. Cassidy, F. Skoulidis, S.A. Ismail, C. Hedberg, M. Hanzal-Bayer, A.R. Venkitaraman, A. Wittinghofer, P.I. Bastiaens, The GDI-like solubilizing factor PDEdelta sustains the spatial organization and signalling of Ras family proteins, *Nat. Cell Biol.* 14 (2011) 148–158.
- [27] Q.S. Wang, K.-H. Zhang, Y. Cui, Z.-J. Wang, Q.-Y. Pan, K. Liu, B. Sun, H. Zhou, M.-J. Li, Q. Xu, C.-Y. Xu, F. Yu, J.-H. He, Upgrade of macromolecular crystallography beamline BL17U1 at SSRF, *Nucl. Sci. Tech.* 29 (2018) 68.
- [28] Z. Otwinowski, W. Minor, Processing of X-ray diffraction data collected in oscillation mode, *Methods Enzymol.* 276 (1997) 307–326.
- [29] A. Vagin, A. Teplyakov, Molecular replacement with MOLREP, *Acta crystallographica, Sect. D, Biol. Crystallogr.* 66 (2010) 22–25.
- [30] G.N. Murshudov, P. Skubak, A.A. Lebedev, N.S. Pannu, R.A. Steiner, R.A. Nicholls, M.D. Winn, F. Long, A.A. Vagin, REFMAC5 for the refinement of macromolecular crystal structures, *Acta crystallographica, Sect. D, Biol. Crystallogr.* 67 (2011) 355–367.
- [31] P.D. Adams, P.V. Afonine, G. Bunkoczi, V.B. Chen, I.W. Davis, N. Echols, J.J. Headd, L.W. Hung, G.J. Kapral, R.W. Grosse-Kunstleve, A.J. McCoy, N.W. Moriarty, R. Oeffner, R.J. Read, D.C. Richardson, J.S. Richardson, T.C. Terwilliger, P.H. Zwart, PHENIX: a comprehensive Python-based system for macromolecular structure solution, *Acta crystallographica, Sect. D, Biol. Crystallogr.* 66 (2010) 213–221.
- [32] P. Emsley, K. Cowtan, Coot: model-building tools for molecular graphics, *Acta crystallographica, Sect. D, Biol. Crystallogr.* 60 (2004) 2126–2132.